A PRELIMINARY ANALYSIS OF THE EFFECTIVENESS OF SECOND HELIUM IONIZATION IN INDUCING CEPHEID INSTABILITY IN STARS

JOHN P. COX
Department of Astronomy and Center for Radiophysics and Space Research, Cornell University
Received January 29, 1960; revised June 13, 1960

ABSTRACT

A program of numerical calculations, carried out by the author, is described and summarized. The purpose of the program was to test the suggestion (Zhevakin 1953, 1954*a*, *b*; Cox and Whitney 1958; Cox 1959) that second helium ionization, occurring at a critical depth in a stellar envelope, is the ultimate source of cepheid instability. All calculations were performed on an IBM 704 electronic computer. Simplified, purely radiative envelope models were adopted for stars of prescribed mass, luminosity, radius, and chemical composition, and the negative dissipation in the envelopes was computed numerically as a function of these parameters. The Woltjer theory in the first approximation was used to obtain the nonadiabatic flux and temperature variations, from which the negative dissipation in the envelopes could be computed. Second helium ionization was explicitly included in the calculations, but first helium ionization and hydrogen ionization were omitted.

A strong destabilizing influence, resulting from second helium ionization, was revealed in the envelope models for population I cepheids, assuming reasonable helium abundances. The magnitude of the negative dissipation in the envelopes was comparable to the estimated positive dissipation in the interiors, for reasonable radii. While no definitive conclusions could thus be drawn concerning the sign of the total dissipation for the entire star, the possibility of pulsational instability is, at any rate, not excluded by these calculations. For log L (solar units) = 3.13 and B (helium/hydrogen ratio, by numbers) = 0.15, *maximum* instability for the entire star was attained for a value of the radius about 1.6 times larger than the empirical value. For these same values of log L and B and for radii near the observed values, the amplitude of the surface flux variations was about $0^m.7$ or $0^m.8$ and the phase lag (relative to minimum radius) was about 40° or 50°; these values may be considered to be very roughly consistent with observations of classical cepheids. It may be inferred from the calculations that, for stars in the cepheid region, first helium ionization and hydrogen ionization are not *primary* causative agents in producing pulsational instability, at least for the kinds of envelopes considered here. These ionizations, however, had they been included in the calculations, would have increased the magnitude of the pulsational instability (through indirect effects) and would have brought the surface flux variations into closer agreement with observation than the present calculations show.

Results for population II cepheids were inconclusive because the low surface gravities of these stars (assuming $M = 1.25\,M_\odot$) invalidated some of the approximations that were used. It is concluded that the results of the calculations are generally favorable to the helium-ionization hypothesis, at least as applied to the population I cepheids. Because of various uncertainties, however, this conclusion must be regarded as tentative.

I. INTRODUCTION

This paper presents a description and a summary of some results obtained from a project begun by the author in the spring of 1959 at Cornell University and concluded during the summer of 1959, while he was acting as a consultant at the Smithsonian Astrophysical Observatory in Cambridge, Massachusetts.

The general purpose of the work to be described here was to effect a quantitative test of the suggestion (Zhevakin 1953, 1954*a*, *b*; Cox and Whitney 1958, hereafter referred to as "Paper IV"; Cox 1959, hereafter referred to as "Paper V") that second helium ionization, occurring at a critical depth in a stellar envelope, is the ultimate source of cepheid instability. The general plan of attack was, first, to adopt simplified envelope models for stars of prescribed mass (M), luminosity (L), radius (R), and chemical composition (in particular, B, helium/hydrogen ratio, by numbers) and, second, to compute numerically, using an approximate linear theory, the negative dissipation and other pulsation properties as functions of these parameters. More specifically, by adopting semiempirical rela-

tions between L and M for both population I and population II cepheids and by supposing a star to evolve with constant L and M, it was planned to determine the range of radii (and hence periods) for which a star with given L and M would be pulsationally unstable. One of the principal results of such a computation, if successful, would be a mapping of regions of cepheid instability on the Hertzsprung-Russell diagram and hence a delineation of the period-luminosity (II-L) relations of cepheids of populations I and II. Comparison of the computed relations with the observed ones was to have provided one test of the helium-ionization theory.

Another result of such a computation would be the determination of the amplitude and phase of the variations in emitted flux (relative to the radial variations) for stars which are pulsationally unstable. Comparison with the observed flux variations of cepheids was to have provided another (but less rigorous) test of the theory.

The scope of the project was such that it could be carried out only with the aid of a fast electronic computer. Preliminary work, including the development and refinement of many of the details of the computational procedure, was carried out by use of the Cornell Computing Center's electronic computer (at that time, an IBM 650) and of the IBM 650 at the Littauer Statistical Laboratory at Harvard University. The final program was written for an IBM 704 electronic computer, and the actual calculations were performed on the 704, which was installed at the Smithsonian Astrophysical Observatory in midsummer of 1959.

A calculation designed to realize the goals outlined above entails two general requirements: (1) a sequence (or sequences) of equilibrium stellar models and (2) a (linear) theory of non-adiabatic pulsation.

To date, satisfactory equilibrium models for cepheids do not exist. Ideas underlying the present approach indicate, however, that most of the physical factors that are of decisive importance in determining pulsational instability operate only in the outer stellar layers, in particular in those regions having temperatures (T) less than, say, about 200000° K. Because the emphasis in this study was to be primarily on the mechanism for exciting the pulsations, it was decided that envelope models alone might suffice for the purposes of this investigation, especially in view of its exploratory nature; and simplified envelope models were accordingly adopted (cf. Sec. II, *a*). A further justification of this approach was provided by the interest in the character of the non-adiabatic flux terms themselves in the extreme outermost layers. The investigation showed that, aside from a single parameter whose value had to be assigned (this was the constant in the period–mzan density relation, cf. eq. [15*a*]), the amplitude and phase of the surface flux variations were determined to within an accuracy of better than 1 part in 10^8 by conditions in the envelopes alone.

A restriction imposed by the lack of interiors is that an accurate computation of the dissipation for the entire star cannot be made. It was planned, however, to estimate the positive dissipation in the interior regions in only an approximate way, since it was anticipated that the negative dissipation in the envelopes would depend rather critically on the stellar radii and would outweigh by a considerable margin the positive dissipation in the interior regions, for reasonable helium abundances and for radii in the appropriate range (cf. Sec. IV, *c*).

The approach adopted for the non-adiabatic problem was the iterative procedure suggested by Woltjer (1936). (For a discussion of this, as well as of certain other matters connected with the non-adiabatic problem, see Cox [1958], hereafter referred to as "N-A I".) The Woltjer method in the first approximation consists in using the solution of the *adiabatic* wave equation to compute the quasi-adiabatic flux variations and their first derivatives, and then using these derivatives in the right-hand sides of the Woltjer "v-equations" (cf. eqs. [34*a*], [34*b*]). The solution of the Woltjer v-equations yields the non-adiabatic flux and temperature variations, from which the negative dissipation in the envelopes can be computed.

The ultimate intention was to attempt to achieve a sufficiently accurate solution of the non-adiabatic problem by proceeding to higher and higher approximations in the iterative procedure. In the course of the summer's work, however, time limitations permitted only the first approximation to be carried through.

It is therefore important to emphasize that the mathematical problem of the non-adiabatic pulsations of the envelopes has not actually been solved in this investigation. The mathematical accuracy of the results obtained by use of the Woltjer method in the first approximation is not really known at present, although certain arguments may be advanced (cf. Sec. V) which suggest that the results are not likely to be grossly incorrect qualitatively.[1] For this reason, many of the precise numerical results of this calculation must be regarded as tentative, even within the framework of the physical approximations that have been made.

II. METHOD OF CALCULATION, PRINCIPAL EQUATIONS USED

a) The Envelope Models

For simplicity and in view of the results reported in Paper V, purely radiative envelope models were adopted. The opacity was approximated by an interpolation formula of the form

$$\kappa = \kappa_0 \rho^n T^{-s} , \tag{1}$$

where ρ is the density, and κ_0, n, and s are constant throughout a particular model envelope; κ_0 is a function of the helium/hydrogen ratio B, given (for $B \geqslant 0.05$), approximately, by

$$\kappa_0 = \kappa_{00} \frac{B}{1+B} , \tag{2}$$

where

$$\log \kappa_{00} = 1.4379 + 7.9676\,(n) + 4.5057\,(s) . \tag{3}$$

The numerical constants in equation (3) were chosen so that equation (1) would provide a reasonable approximation to tabulated opacities at some representative point in the envelopes.

Radiative envelopes with opacity given by equation (1) have a polytropic structure (provided that $M_r \approx M$, $L_r \approx L$, and μ [mean molecular weight] = const.; cf. Schwarzschild 1958, pp. 90–92), so that the relation between pressure P and temperature T is

$$P = K_{n_e} T^{n_e+1} , \tag{4}$$

where

$$n_e \equiv \frac{s+3}{n+1} \tag{5}$$

is the effective polytropic index and

$$K_{n_e} \equiv \left[\frac{16\pi a\, cG}{3\kappa_0 (n_e+1)} \left(\frac{L}{M}\right) \left(\frac{k}{\bar{\mu} H}\right)^n \right]^{1/(1+n)} . \tag{6a}$$

Here a, c, G, k, and H are, respectively, the radiation constant, the velocity of light *in vacuo*, the gravitation constant, Boltzmann's constant, and the reciprocal of Avogadro's number, and $\bar{\mu}$ is the value of the mean molecular weight at a representative point in the envelope. We may also write equation (6*a*) in the form

$$\log K_{n_e} = \frac{1}{n+1} [-9.8837 + 7.9198n - \log (n_e+1) + \log M - \log L - \log \kappa_0 - n \log \bar{\mu}] , \tag{6b}$$

[1] See footnotes at end of Section V.

where L and M are in solar units (as they are throughout the present paper). The representative point for the evaluation of $\bar{\mu}$ was taken to lie in the region between the zones of first and sesond helium ionization; hence $\bar{\mu}$ is given (neglecting elements heavier than helium) by

$$\bar{\mu} = \frac{1+4B}{2(1+B)}. \tag{7}$$

The temperature distribution in the polytropic envelopes is given by

$$T = Dz, \tag{8}$$

where

$$z \equiv \frac{1}{x} - 1, \tag{9}$$

$$x \equiv \frac{r}{R}, \tag{10}$$

and

$$D \equiv \frac{1}{n_e+1}\frac{GH}{k}\frac{\bar{\mu}M}{R} = \frac{22.94\times 10^6}{n_e+1}\frac{\bar{\mu}M}{R}\,^\circ\mathrm{K}, \tag{11}$$

where R is also in solar units, as it is throughout this paper.

It can be shown that the values of z at which the photospheric density is reached are much less than 1 for all the population I cepheid models considered here and for the population II cepheid models having periods less than, say, about 10 days. Hence, for these models, the "radiative zero" solution (Schwarzschild 1958, pp. 90–92) expressed by equation (4) is an adequate approximation (cf. also Hoyle and Schwarzschild 1955).

b) Method of Treatment of the Adiabatic Problem

In accordance with the discussion in Section I, the first step in the Woltjer scheme is to obtain the solution of the adiabatic wave equation for the envelopes. Since the Woltjer method is an iterative procedure, it was deemed permissible to introduce some simplifications into this first step. To facilitate convergence, however, the simplified treatment should nevertheless be reasonably accurate. Accordingly, the solutions of the adiabatic wave equation (in the fundamental mode, the only one considered) were approximated by the analytical solutions, expressible in terms of Bessel functions, for plane-parallel, polytropic envelopes (Rosseland 1949, pp. 24 ff.), modified to take into account, in an approximate way, the curvature of the envelopes. Explicitly, the relative pulsation semiamplitude (normalized to unity at the surface and assumed purely real) was approximated by the relation

$$y = \frac{2^{n_e}\Gamma(n_e+1)}{x}\frac{J_{n_e}(\zeta)}{\zeta^{n_e}}, \tag{12}$$

where $J_{n_e}(\zeta)$ is the Bessel function of the first kind, of order n_e, and Γ denotes the gamma function; ζ is defined by the relation

$$\zeta \equiv 2\Omega\left(\frac{n_e+1}{\Gamma_1}\right)^{1/2}(1-x)^{1/2}, \tag{13}$$

where Γ_1 is the appropriate effective ratio of specific heats (assumed constant) and

$$\Omega^2 \equiv \frac{\sigma^2 R^3}{GM} \tag{14a}$$

$$= 8.3938\left(\frac{0.04}{Q_d}\right)^2. \tag{14b}$$

The factor x^{-1} in equation (12) takes curvature into account in an approximate way. In equation (14*a*), σ denotes the (real) adiabatic pulsation eigen-frequency. Equation (14*b*) follows from equation (14*a*) by making use of the period–mean-density relation,

$$\Pi M^{1/2} R^{-3/2} = Q \,, \tag{15a}$$

where Π is the adiabatic pulsation period and a subscript d means that the units are in days. If $Q_d = 0.04$, equation (15*a*) may be written in the form

$$\log R = 0.932 + \tfrac{1}{3} \log M + \tfrac{2}{3} \log \Pi_d \,. \tag{15b}$$

The lack of interiors has the consequence that central boundary conditions cannot be used to determine the adiabatic pulsation periods. Therefore, a suitable semiempirical value of Q was used for most of the calculations, and some calculations were performed by using altered values of this constant, to determine their effects (cf. Sec. IV, *e*).

Comparison with published integrations shows that equation (12) (with the appropriate value of Ω or Q) reproduces the actual integrations to within, generally, better than about 10 per cent in the regions of greatest interest (say $x \gtrsim 0.9$). In the deeper regions, however, equation (12) may be a poor representation of the relative pulsation amplitude, for two reasons. First, the curvature correction (the factor x^{-1}) is probably inadequate. Second, and perhaps more important, are the indirect effects introduced by the absence of interiors. The absence of interiors precludes accurate knowledge of the mathematically correct value of Q, and the relative pulsation amplitude is quite sensitive to the value of Q in these deeper regions (cf. Sec. IV, *e*).

Such a treatment as this neglects the effects of ionization on the adiabatic pulsations; these effects, however, were not considered important in a first approximation. It was planned to carry through subsequent approximations without making use of these simplifications.

In the computation of the quasi-adiabatic flux variations in the envelopes (cf. eq. [35]), second ionization of helium was taken explicitly into account, although first helium ionization and hydrogen ionization were omitted. The principal reason for the omission of these last two ionizations was that rough computations had indicated that their inclusion would have only a minor effect on the solution of the non-adiabatic problem. Moreover, inclusion of these additional ionizations would have increased the complexity of the numerical calculations by a large factor. As it turned out (cf. Sec. IV), the indirect effects of these additional ionizations were more serious than had been anticipated.

The effect of second helium ionization manifests itself predominantly through its influence on the value of the effective ratio of specific heats (Γ_3); the effect on the values of the exponents n and s was found to be small and so was neglected. Consequently, the run of values of Γ_3 throughout each envelope was accurately computed (cf. Table 2*A*). Values of the first and second derivatives with respect to temperature (i.e., position) were also required. Because, for reasons that will be given in Section II, *c*, accurate values for these derivatives were needed, they were computed from rather involved analytical formulae. For completeness and for possible future reference, the runs of the other gammas (Γ_1 and Γ_2) were also computed for each envelope. The effects of second helium ionization also appear in the coefficients of the v-equations (i.e., in h_2, cf. eqs. [31] and [33]); these effects were accurately included in the calculations.

The gammas were computed from the formulae

$$\Gamma_1 \equiv \left(\frac{d \ln P}{d \ln \rho}\right)_{\rm ad} = \frac{5 + \Xi (2.5 + 125.3\theta)^2}{3 + \Xi [(1.5 + 125.3\theta)(2.5 + 125.3\theta) - 125.3\theta]} \,, \tag{16}$$

$$\Gamma_3 - 1 \equiv \left(\frac{d \ln T}{d \ln \rho}\right)_{\rm ad} = \frac{2 + \Xi (2.5 + 125.3\theta)}{3 + \Xi [(1.5 + 125.3\theta)(2.5 + 125.3\theta) - 125.3\theta]} \,, \tag{17}$$

and

$$\frac{\Gamma_2}{\Gamma_2-1}\equiv\left(\frac{d\ln P}{d\ln T}\right)_{\rm ad}\equiv\frac{\Gamma_1}{\Gamma_3-1}, \tag{18}$$

where

$$\theta\equiv\frac{5040.3}{T} \tag{19}$$

and

$$\Xi\equiv\frac{2\eta(1-\eta)B[1+B(1+\eta)]}{[1+B(1+\eta)][2+B(2+\eta)]+\eta(1-\eta)B(1+B)}. \tag{20}$$

Here η is the degree of second helium ionization (the fraction of all helium atoms and ions that are twice ionized), given by the Saha equation; for polytropic envelopes, this may be written in the form

$$\log\left[\frac{\eta}{1-\eta}\frac{1+B(1+\eta)}{2+B(2+\eta)}\right]=-0.4772-\log K_{n_e}-3.7024(n_e-1.5)+(n_e-1.5)\log\theta-54.40\theta. \tag{21}$$

The derivatives of Γ_3-1 were obtained by analytical differentiation of equations (17), (20), and (21). Equations (16), (17), and (20) are approximately valid if only two successive stages of ionization of one element are effectively in progress, as is assumed to be the case here (hydrogen ionization and first helium ionization are assumed to be complete); these equations may be derived in a manner analogous to that used, for example, by Unsöld (1955). The relation between the three gammas expressed by equation (18) is an identity that is generally valid.

c) *The Woltjer v-Equations*

Before presenting the Woltjer v-equations, we must explain the notation used. In general, the normalized Lagrangian variation of any physical quantity, f, is written as

$$\frac{\delta f}{\eta_0 f}\equiv f_\kappa e^{i\sigma' t}, \tag{22}$$

where f_κ is the complex amplitude of the relative variation and

$$\sigma'=\sigma+i\kappa \tag{23}$$

is the complex angular pulsation frequency, where σ is the adiabatic eigen-frequency, and κ is the (complex) stability coefficient (cf. Rosseland 1949, chap. v); f_κ is a function only of x and $\eta_0\equiv|\delta R/R|$ is the absolute value of the relative pulsation semiamplitude at the surface of the star. In terms of real and imaginary parts, we write

$$-f_\kappa=f_1+if_2, \tag{24}$$

where f_1 and f_2 are real. For the (normalized) relative pulsation amplitude itself, we write

$$y_\kappa=y_1\equiv y, \tag{25}$$

since $y_2=0$ in the present approximation (corresponding to standing-wave solutions).

The Woltjer v-equations as used here may be derived by means of the relation

$$T_\kappa=(\Gamma_3-1)\rho_\kappa+v_\kappa \tag{26}$$

in the expression for H_κ, the variation in the net rate of flow of energy H (here purely radiative) through a sphere of radius r. Here ρ_κ is the relative density variation, given by

$$-\rho_\kappa = 3y_\kappa + xy'_\kappa , \tag{27}$$

where a prime denotes differentiation with respect to x, and v_κ is the non-adiabatic contribution to the temperature variation. We may write H_κ in the form

$$H_\kappa = \mathfrak{H}_{\kappa,a} + V_\kappa , \tag{28}$$

where $\mathfrak{H}_{\kappa, a}$, the quasi-adiabatic flux variation, contains all terms which do not depend explicitly on v_κ or v'_κ and where

$$V_\kappa = (s+4)\, v_\kappa + z\frac{dv_\kappa}{dz} \tag{29}$$

is the non-adiabatic contribution to the flux variation. (Note that $\mathfrak{H}_{\kappa, a}$ and V_κ are here defined differently than in N-A I.) In regions in which there is no energy production, the energy equation may be written in the form

$$\frac{dH_\kappa}{dz} = ih_2 x^2 v_\kappa , \tag{30}$$

where

$$h_2 = \frac{4\pi R^3 \sigma}{L} c_v \rho T x^2 , \tag{31}$$

c_v being the specific heat per unit mass at constant volume. Defining

$$\Theta_T \equiv \frac{P}{c_v \rho T} \tag{32}$$

and using equation (4), we may also write equation (31) in the form

$$h_2 = \frac{4\pi R^3 \sigma K n_e}{L\Theta_T} T^{n_e+1} x^2 . \tag{33}$$

Substituting equations (28) and (29) in equation (30) yields the Woltjer v-equations, which may be written (for n and s constant), in terms of real and imaginary parts, as

$$\frac{d^2 v_1}{dz^2} + \frac{s+5}{z}\frac{dv_1}{dz} + \frac{h_2 x^2}{z} v_2 = \frac{x^2}{z}\mathfrak{H}'_{1, a} , \tag{34a}$$

$$\frac{d^2 v_2}{dz^2} + \frac{s+5}{z}\frac{dv_2}{dz} - \frac{h_2 x^2}{z} v_1 = 0 . \tag{34b}$$

For polytropic envelopes in radiative equilibrium, we have

$$\mathfrak{H}_{1, a} = -4y - \left[n - T\frac{d(\Gamma_3 - 1)}{dT}\right]\rho_1 + [(s+4)\rho_1 - zx^2\rho'_1](\Gamma_3 - 1) , \tag{35}$$

where y, ρ_1, and ρ'_1 are to be computed from the solution of the adiabatic wave equation. The right-hand side of equation (34b) is zero in the present approximation because $y_2 = 0$.

It is seen that the effects of curvature, which were taken into account in only an approximate way in the solutions of the adiabatic wave equation, have been allowed for exactly in the v-equations.

Equations (34*a*) and (34*b*) were integrated numerically for each model envelope, with surface boundary conditions appropriate to vanishing temperature and density (i.e., $z \rightarrow 0$). Satisfaction of these boundary conditions requires that each integration be started at the surface and carried inward. The surface boundary conditions suffice, however (as may be seen from eqs. [34*a*] and [34*b*]), to determine only two of the four constants of integration; the remaining two must be determined by the requirement that the solutions of the v-equations remain finite in the deep interior (from the standpoint of the v-equations, the "deep interior" is still well within the envelope, say in regions with $T > 80000°$ K; this is due to the extremely rapid rate of increase of h_2 inward). Consequently, the numerical solution of the v-equations is of the nature of a double eigen value problem, and a series of trial integrations is required, for each model, to determine the values of the two remaining constants of integration. Explicitly, these two constants of integration are the surface values of V_1 and V_2 (or v_1 and v_2). An extremely efficient, fully automatic searching procedure was evolved, by means of which the surface values of V_1 and V_2 could be determined to within better than 1 part in 10^8 in only twelve to eighteen trial integrations. The method of integration and the searching procedure will be described in Sections III, *b* and *c*, respectively.

A comment is in order concerning the very high accuracy to which the surface values of V_1 and V_2 were computed. Such great accuracy is, of course, not essential if one is interested only in the surface flux variations themselves. However, in evaluating the stability coefficient for the envelopes, an integration through the envelopes is required, using the solutions of the v-equations (cf. Secs. III, *a*, and IV, *c*). Consequently, these solutions must be reasonably accurate throughout the major portion of the envelopes. Now an analytical study of the v-equations shows that any error in the starting values of V_1 and V_2 increases inward very rapidly, a behavior which was subsequently confirmed by the numerical work. Hence, at levels in the "deep interior" (say $T \approx 100000°$–$150000°$ K), the error in the surface values of V_1 and V_2 will have been multiplied by a factor of about 10^4–10^6. In addition, at these levels the magnitudes of V_1 and V_2 themselves will have decreased, typically, by factors of about 10^{-2}–10^{-4} below their surface values. It therefore appeared that if all calculations were carried to eight significant figures (the capacity of the machine with single precision), it would be possible to carry the integrations through the significant portions of the envelopes and on down to these levels in the "deep interior" without having to use special procedures to continue the integrations. Working to eight significant figures, the maximum depth to which it was actually possible to carry any final integration (without using special procedures) was about $T = 170000°$ K; in some cases the final integration could be carried only to about $T = 90000°$ K. (This maximum depth is the depth at which the solutions begin to diverge because of numerical inaccuracies in the surface values of V_1 and V_2.) This emphasis on numerical accuracy and the desirability of having a smooth function for $\mathfrak{H}'_{1,a}$ explain why the derivatives of $\Gamma_3 - 1$ were evaluated analytically rather than by numerical differentiation.

d) Analytic Theory of the Woltjer v-Equations

An analytic study of the Woltjer v-equations was carried out by the author, in part to serve as a guide for the numerical work. While the details of this study are much too elaborate to be presented here, it is felt that, since the results of this study have been used to extend and check some of the numerical results of the present calculations (cf. Secs. IV and III, *b*), at least a descriptive outline of the study should be given.

For the case of plane-parallel, polytropic envelopes in radiative equilibrium, it was found possible, by means of suitable transformations of variables, to express the solution of the homogeneous, transformed (complex) v-equation in terms of cylinder functions of real order and complex argument. With these solutions of the homogeneous equation available, it was then possible, by using well-known procedures (cf., e.g., Forsyth 1929), to write down the formal solution of the transformed, inhomogeneous v-equation (the

inhomogeneous part of this equation depends on $\mathfrak{H}_{\kappa,\,a}$, the quasi-adiabatic flux variation). The formal solution was then applied to some schematic $\mathfrak{H}_{\kappa,\,a}$-curves (assumed given).

It was found that the integrals in the formal solution could be evaluated explicitly (again in terms of cylinder functions) for the case in which the $\mathfrak{H}_{\kappa,\,a}$-curve (considered as plotted against ϕ; cf. eq. [37]) was made up of a series of straight-line segments. For generality, the number of straight-line segments was left arbitrary, and the possibility of discontinuities in the $\mathfrak{H}_{\kappa,\,a}$-curve was allowed for (see N-A I, Sec. IV, *c*, for an example of such a discontinuity). The discontinuities which occur both in $\mathfrak{H}_{\kappa,\,a}$ and in its slope in such an "*n*-zone model" were dealt with by use of the Dirac delta function. The constants of integration were evaluated explicitly by application of appropriate boundary conditions at the surface and in the "deep interior." Explicit equations were thus derived for computing the solution V_κ which satisfies all the boundary conditions at any point (including the surface) in such an *n*-zone model. Because of the complexity of these equations, they will not be presented here.

Since the number of zones was left arbitrary, the analytic solution so obtained could be used, in principle, to calculate the solution V_κ associated with an arbitrary $\mathfrak{H}_{\kappa,\,a}$-curve to any desired degree of accuracy by taking the number of zones to be sufficiently large. In practice, however, the labor of computation required to evaluate the analytic solution numerically with a large number of zones would probably be greater than that required by purely numerical methods. In addition, the usefulness of the analytic solution is limited, even in principle, for highly accurate work because curvature in the envelopes and the effect of ionization on the function h_2 (cf. eqs. [31] and [33]) are both neglected in the analytic theory, whereas these effects are included in the numerical work.

The specific cylinder functions employed were the Bessel function of the first kind, $J_\nu(\xi)$, and the Hankel function of the third kind, $H_\nu^{(1)}(\xi)$, where $\xi \propto i^{3/2}\phi^{1/2}$, ϕ being defined by equation (37), and where ν, a real number, is a function of the exponents n and s in the opacity law (eq. [1]). These functions form a fundamental system of solutions of Bessel's equation for all values of ν (cf. Watson 1944). Because of this choice of cylinder functions, the equations for V_1 and V_2, the real and imaginary parts of $-V_\kappa$, are expressible in terms of the ber $_\nu$, bei $_\nu$, her $_\nu$, and hei $_\nu$ functions discussed by Whitehead (1911).

In the specific application of the analytic theory made here, it was found that the $\mathfrak{H}_{1,\,a}$-curves could be adequately represented by a three-zone model; when $\mathfrak{H}_{1,\,a}$ is plotted against ϕ for a typical envelope, the three principal portions of the curve approximate rather closely straight-line segments (cf. Fig. 2). In view of the close correspondence between the results obtained from the numerical work and from the analytic theory (cf. Sec. III, *b*), it may be concluded that the approximations involved in the analytic theory do not lead to appreciable errors.

III. ACTUAL CALCULATIONS

a) General

The actual calculation, programed for and carried out on an IBM 704 electronic computer, was divided into three major parts, as follows: Part I: construction of model envelopes; Part II: solution of adiabatic wave equation and evaluation of coefficients of v-equations; and Part III: solution of v-equations and evaluation of stability coefficient.

The parameters which entered into Part I were L, M, n, s, and B. Two semiempirical mass-luminosity relations were used, one for population I cepheids and one for population II cepheids. These were as follows:

$$\text{Population I: } \log M = 0.304 \log L - 0.220 \; ; \tag{36a}$$

$$\text{Population II: } \quad M = 1.25, \text{ all } L \, . \tag{36b}$$

Equation (36*a*) is based on semitheoretical evolutionary arguments and is obtained from equation (5) of Sandage (1958) by taking $M_{\rm bol}\,(\odot) = 4.77$; this value follows from the values of the solar absolute photovisual magnitude given by Stebbins and Kron (1957) and the bolometric correction given by Kuiper (1938). In this part were computed, principally, the degree of second helium ionization (from eqs. [21] and [6*b*]); Γ_1, Γ_2, and Γ_3 (from eqs. [16] through [20]); and the first and second derivatives of Γ_3, all as functions of T. Each envelope went from $T = 0°$ K to $T = 200000°$ K, in steps of $\Delta T = 100°$.

The additional parameters required for Parts II and III were R and Q; the value of Γ_1 in equation (13) was taken as $\frac{5}{3}$ for all models. In Part II were computed, for each R and Q, the geometrical depth, z, in the envelopes, as a function of T (from eqs. [8] and [11]); the Bessel function solutions of the adiabatic wave equation (from eqs. [12], [13], and [14]) and their appropriate derivatives; the quasi-adiabatic flux variations, $\mathfrak{H}_{1,\,a}$ (from eq. [35]) and their first derivatives (by analytical differentiation of eq. [35]); the coefficients of the v-equations (cf. eqs. [31], [33], and [34*a*], [34*b*]); the phase-lag function (introduced and discussed in N-A I and Papers IV and V), given in the present notation by

$$\phi\,(z) = \int_0^z \frac{h_2 x^2}{s + 4}\, dz' \tag{37}$$

(note that eq. [37] includes curvature), as well as several other relevant quantities.

Part III involved, for each R and Q, the solution of the v-equations and the evaluation of the stability integral for the envelopes. The automatic searching procedure (cf. Sec. III, *c*) was programed into Part III. The machine would do successive trial integrations (each going to $T = 200000°$ K) until the surface values of V_1 and V_2 had been found to within the accuracy limitations of the machine, and then would proceed to perform the final integration, which included calculation of the contribution of the envelopes to the stability coefficient, as well as of numerous other subsidiary quantities. For each model an average of about fifteen trial integrations was required to yield the starting values of V_1 and V_2 to an accuracy of eight significant figures. In the final integration, an automatic stopping procedure stopped the integration at the point at which the first indications of divergence of the solutions appeared.

The contribution of the regions exterior to z to the real (κ_1) and imaginary (κ_2) parts of the stability coefficient were computed, respectively, from the equations

$$I_1(0,\,z) \equiv \int_0^z \Theta_P \rho_1 \left(-\frac{dH_1}{dz}\right) dz\,, \tag{38a}$$

$$I_2(0,\,z) \equiv \int_0^z \Theta_P \rho_1 \left(-\frac{dH_2}{dz}\right) dz \tag{38b}$$

(cf. Rosseland 1949, chap. v, or N-A I), where, for this problem,

$$\Theta_P = \Gamma_3 - 1 \tag{38c}$$

(cf. N-A I, eq. [20]) and ρ_1 is the relative density variation corresponding to adiabatic oscillations.

For a star of given L, M, R, and Π, $\kappa_1\,(z) \propto I_1\,(0, z)$ and $\kappa_2\,(z) \propto I_2\,(0, z)$. The factors of proportionality cannot be computed accurately without interiors; however, this is not important, as the *sign* of κ_1 is the quantity of interest for stability considerations. A negative value of $\kappa_1\,(z)$ (or $I_1\,[0, z]$) means that the regions exterior to z are exerting a destabilizing influence on the pulsations. The star will be pulsationally unstable if κ_1 for the entire star or if

$$I_1(0, \infty) = I_1(0, z) + I_1(z, \infty) \tag{38d}$$

is negative. Because of the absence of interiors, the values of $I_1\,(z, \infty)$ must be estimated in an approximate way (cf. Sec. IV, *c*).

b) The Method of Integration

The method that was used for the integration of the v-equations (34*a*) and (34*b*) may be explained in general terms by considering a kth-order system of differential equations; this system is equivalent to a single differential equation of the kth order, which we write in the form

$$\frac{d^k w}{dx^k} = f_1\left[\frac{d^{k-1}w}{dx^{k-1}}, \frac{d^{k-2}w}{dx^{k-2}}, \ldots, w; x\right]. \tag{39}$$

(Note that the reduction to a single differential equation has been effected here merely for ease of exposition.) Assuming that w, dw/dx, . . . , $d^k w/dx^k$ are all known at x, we proceed to the point $x + h$ by using the following simple integration formulae:

$$\left(\frac{d^{\lambda-1}w}{dx^{\lambda-1}}\right)_{x+h} = \left(\frac{d^{\lambda-1}w}{dx^{\lambda-1}}\right)_x + \frac{h}{2}\left[\left(\frac{d^\lambda w}{dx^\lambda}\right)_x + \left(\frac{d^\lambda w}{dx^\lambda}\right)_{x+h}\right] \qquad (\lambda = 1, \ldots, k), \tag{40}$$

where the terms neglected in each equation are of order h^3.

The usual procedure for solving equations (39) (evaluated at $x + h$) and (40) for the $k + 1$ unknowns w, . . . , $d^k w/dx^k$ at $x + h$ is by iteration (cf., e.g., Schwarzschild 1958, pp. 119–20). We have chosen, however, to solve equations (39) (evaluated at $x + h$) and (40) *algebraically*, so as to obtain an analytic expression of the form

$$\left(\frac{d^k w}{dx^k}\right)_{x+h} = f_2\left[\left(\frac{d^k w}{dx^k}\right)_x, \left(\frac{d^{k-1}w}{dx^{k-1}}\right)_x, \ldots, w(x); x + h; h\right], \tag{41}$$

all quantities on the right-hand side of which are known. Note that $f_2 \to f_1$ as $h \to 0$; this therefore serves as a rough first check on the algebra. The integration formulae (40) are then applied successively to obtain $(d^{k-1}w/dx^{k-1})_{x+h}$, . . . , $w\,(x + h)$, thus completing the integration from x to $x + h$.

The above algebraic method of solution is therefore exactly equivalent, mathematically, to the iterative method and, of course, yields the same accuracy; consequently, a very small step length must be used (one such that terms of order h^3 are negligible).

The algebraic method possesses the following advantages over the iterative method:

1. The algebraic method enables one to integrate under conditions for which the iterative method will not converge. Such conditions may obtain, for example, in regions in which $d^k w/dx^k$ is poorly determined by the differential equations, as in the vicinity of a singularity of the differential equations. The algebraic method has also been found to work in cases in which the Runge-Kutta method failed.

2. At least for the kinds of singularities met with in the differential equations used here (cf. eqs. [34*a*], [34*b*]), the algebraic method permits one to start integrating right from a singularity, without the necessity of developing the solution about the singularity. The quantities needed in equation (41) *at* the singularity may be obtained by evaluating equation (39) and its higher derivatives at this point. The variety of types of differential equations for which the integration can be begun at a singularity in the way described has not been investigated in detail by the author, but it is suspected that the method will work at least for linear differential equations which possess no essential singularities.

3. In this particular problem the algebraic method was found to be easier to program than the iterative method and required less computing time with the equipment that was used.

The principal disadvantage of the method is that the algebraic manipulation that is required may become rather heavy. It should also be noted that the method will not improve the accuracy of the derivatives if they are poorly determined by the differential equations. The effects introduced by inaccurate values of the derivatives must be checked by some other means.

For the particular problem dealt with here, it was found that a step length of $\Delta T = 100°$ was sufficiently small; so this step length was used in all the integrations.

The algebraic method, as applied to the Woltjer v-equations (34*a*), (34*b*) yields the following equations:

$$\left(\frac{d^2 v_1}{d z^2}\right)_{z_{n+1}} = \frac{1}{C_{n+1}^2 + D_{n+1}^2} \{C_{n+1} [R_{1,\,n+1} - (P_{n+1} B_{1,\,n} + Q_{n+1} A_{2,\,n})] + D_{n+1} [P_{n+1} B_{2,\,n} - Q_{n+1} A_{1,\,n}] \}, \tag{42a}$$

$$\left(\frac{d^2 v_2}{d z^2}\right)_{z_{n+1}} = \frac{1}{C_{n+1}^2 + D_{n+1}^2} \{ D_{n+1} [R_{1,\,n+1} - (P_{n+1} B_{1,\,n} + Q_{n+1} A_{2,\,n})] - C_{n+1} [P_{n+1} B_{2,\,n} - Q_{n+1} A_{1,\,n}] \}, \tag{42b}$$

where

$$P \equiv \frac{s+5}{z}, \qquad Q \equiv \frac{h_2 x^2}{z}, \qquad R_1 \equiv \frac{x^2 \mathfrak{H}'_{1,\,a}}{z}, \tag{43a, b, c}$$

$$C_{n+1} \equiv 1 + \frac{\delta z}{2} P_{n+1}. \tag{44a}$$

$$D_{n+1} \equiv Q_{n+1} \left(\frac{\delta z}{2}\right)^2, \tag{44b}$$

and

$$A_{1,\,n} \equiv v_1(z_n) + (\delta z)\left(\frac{d v_1}{d z}\right)_{z_n} + \left(\frac{\delta z}{2}\right)^2 \left(\frac{d^2 v_1}{d z^2}\right)_{z_n}, \tag{45a}$$

$$B_{1,\,n} \equiv \left(\frac{d v_1}{d z}\right)_{z_n} + \left(\frac{\delta z}{2}\right)\left(\frac{d^2 v_1}{d z^2}\right)_{z_n}, \tag{45b}$$

where $A_{2,\,n}$ and $B_{2,\,n}$ are also given by equations (45*a*) and (45*b*), but with the subscript 1 replaced by 2. The integrations were started right from the surface ($z = 0$). The surface values of the first and second derivatives of v_1 and v_2 were obtained by evaluating equations (34*a*) and (34*b*) and their first derivatives at $z = 0$ and using the condition that v_1 and v_2, as well as their first, second, and third derivatives, be finite here (this procedure is equivalent to evaluating the first three terms in the expansions of v_1 and v_2 about $z = 0$). Because the second derivatives are poorly determined by equations (42*a*) and (42*b*) for z very small, several significant figures in these derivatives were lost at the first step ($T = 100°$). However, since the calculation was carried out with eight-figure accuracy, these derivatives were still good to four or five significant figures at this point and were continuous with the surface values of the derivatives. (Indeed, it may be shown that, in the limit of vanishing step length, the values of the second derivatives, as given by eqs. [42*a*] and [42*b*], must be continuous with the surface values at the first integration step, in spite of the singularities in the coefficients.) After two successive integrations, for each of v_1 and v_2, by use of formulae of the form of equations (40), the lost figures had been regained, so that v_1 and v_2 themselves were again accurate to eight significant figures at this point. In addition, because of the smallness of the factors multiplying the second derivatives in equations (45*a*) and (45*b*), high accuracy in these derivatives is not essential in integrating to the next step.

Two checks were applied to insure that the procedure for starting the integrations and the loss of significant figures in $d^2 v_{1,\,2}/dz^2$ for small z had not introduced any severe inaccuracies into the final results or led to a wrong solution.

First, a power-series solution of equations (34*a*) and (34*b*) was obtained by expanding $\mathfrak{H}'_{1,\,a}$ in a Taylor series about $z = 0$, and a few terms in the expansions for v_1 and v_2 were

evaluated for a typical model envelope. The values of v_1 and v_2, computed in this manner, were then compared with the values obtained by the numerical integration at some small value of T, and the two sets of values showed very close agreement.

(This power-series development was considered impractical for general use in beginning the integrations because the series coefficients involve increasingly higher derivatives of $\mathfrak{H}'_{1,a}$ and the evaluation of derivatives of $\mathfrak{H}'_{1,a}$ higher than the second or third becomes excessively laborious. In addition, the magnitudes of the successive coefficients were found to increase rather rapidly, so that a fairly large number of terms would have been required to reach a value of z such that a standard integration procedure could be used with confidence. This difficulty, together with the fact that a development in the simple form considered here is possible only for integral values of n_e, was largely responsible for the decision to use the algebraic method described above.)

Second, the analytic theory outlined in Section II, *d*, was applied to calculate the correct surface values of V_1 and V_2 for a typical envelope model (Model 1, cf. Sec. IV, *a*), by using a three-zone model for the $\mathfrak{H}_{1,a}$-curve (cf. Fig. 2). Comparison with the corresponding values of V_1 and V_2 as obtained from the numerical work showed that the two sets of values differed from each other by only a few per cent; this is as good an agreement as can be expected in view of the approximations which were involved in the analytic theory. It therefore seems safe to conclude that no appreciable errors were introduced into the final results and that no wrong solutions were obtained by the particular method of integration that was used.

c) The Automatic Searching Procedure

The automatic searching procedure that was used for the determination of the correct surface values of V_1 and V_2 was based on the following simple considerations. Let $\Delta V_{1,2}(T_c)$ denote the changes in V_1 and V_2 at some fixed temperature, T_c, due to the changes $\Delta V_{1,2}(0)$ in V_1 and V_2 at the surface ($T = 0$). We then assume the following linear relation to be valid:

$$\Delta V_i(T_c) = \sum_{j=1}^{2} a_{ij}(T_c)\,\Delta V_j(0) \qquad (i = 1, 2), \tag{46}$$

where

$$a_{ij}(T_c) \equiv \frac{\partial V_i(T_c)}{\partial V_j(0)} \qquad (i, j = 1, 2). \tag{47}$$

Solving equation (46), we obtain

$$\Delta V_1(0) = \frac{a_{22}\Delta V_1(T_c) - a_{12}\Delta V_2(T_c)}{a_{11}a_{22} - a_{12}a_{21}} \tag{48a}$$

and

$$\Delta V_2(0) = \frac{a_{11}\Delta V_2(T_c) - a_{21}\Delta V_1(T_c)}{a_{11}a_{22} - a_{12}a_{21}}. \tag{48b}$$

It can be shown from analytic considerations that, in this problem, the relation between $\Delta V_{1,2}(T_c)$ and $\Delta V_{1,2}(0)$ is, in principle, strictly linear or that the $a_{ij}(T_c)$'s are strictly independent of $V_{1,2}(0)$. This, in fact, accounts in part for the rapidity of convergence of the method in this case. In practice, however, because of small numerical inaccuracies, the $a_{ij}(T_c)$ showed a slight, erratic dependence on $V_{1,2}(0)$, so that, to secure the high accuracy that was desirable (cf. Sec. II, *c*), a searching procedure was required.

The values of $\Delta V_{1,2}(T_c)$ can be found from a single integration at any stage in the approximation from knowledge of the required behavior of $V_{1,2}$ in the "deep interior"

(cf. Sec II, *c*) where T_c is located. If T_c is such that $\phi(T_c) \gg 1$ (cf. eq. [37]) (this is, in fact, the condition that T_c be in the "deep interior"), then it is known (cf. last paragraph in Sec. IV, *a*) that the physically correct solution is that one for which $|V_{1,2}(T_c)| \ll 1$; in practice, it was found that $V_{1,2}(T_c) = 0$ provided an adequate approximation. The values of the $a_{ij}(T_c)$'s can be found from two additional integrations, at the same stage in the approximation, by replacing the right-hand side of equation (47) by the corresponding ratio of two finite differences.

At each stage in the approximation, three points in the $V_{1,2}(0)$ plane were selected, say *a*, *b*, and *c*, as indicated in the following scheme:

$$a\text{:}\quad V_1^{(a)}(0)\,, \qquad V_2^{(a)}(0)\,;$$

$$b\text{:}\quad V_1^{(a)}(0) + \Delta\,, \qquad V_2^{(a)}(0)\,;$$

$$c\text{:}\quad V_1^{(a)}(0)\,, \qquad V_2^{(a)}(0) + \Delta\,,$$

where Δ denotes the "grid size" assosiated with the triad of integrations carried out at each stage. Point *a* is the point whose location had been predicted in the preceding stage. The magnitude of Δ was computed at each stage so as to facilitate convergence. Experience had shown that convergence would be most rapid, for this problem, if the magnitude of Δ for each stage were chosen to be about an order of magnitude larger than the value which would be predicted in that stage for the change in $|V_{1,2}(0)|$.

The actual searching procedure then was as follows: In the kth stage of approximation, the first step was to carry out a single integration at point *a*, whose location had been predicted in the $(k = 1)$th stage of approximation. Because only a single integration is needed to determine $\Delta V_{1,2}(T_c)$, a rough estimate could be made of the values of $\Delta V_{1,2}(0)$ by using the values of the $a_{ij}(T_c)$ as computed *in the* $(k - 1)$*th stage of approximation* in equations (48*a*) and (48*b*). From these rough values, the new grid size for the kth stage could then be computed. The actual relation used was

$$\Delta^{(k)} = A\sqrt{\left\{\frac{[\Delta V_1^{(k)}(T_c)]^2 + [\Delta V_2^{(k)}(T_c)]^2}{[a_{11}^{(k-1)}a_{22}^{(k-1)} - a_{12}^{(k-1)}a_{21}^{(k-1)}]_{T_c}}\right\}}\,, \tag{49}$$

where A is an arbitrary constant which was set equal to 10 in these calculations. Once $\Delta^{(k)}$ had been determined, the locations of the points *b* and *c* were then known, and the remaining two integrations for the kth stage could be carried out. From these three integrations, the values of the $a_{ij}^{(k)}(T_c)$, for the kth stage, could be computed from equations (47), and a new point *a*, for the $(k + 1)$th stage, could be predicted from equations (48*a*) and (48*b*). The process was continued either until the predicted changes in $V_{1,2}(0)$ fell below the accuracy criterion or until the computed value of Δ for a given stage of approximation had become larger than that in the preceding stage (at which time the limiting accuracy of the searching procedure had been reached). The final integration was then performed, using the best predicted values of $V_{1,2}(0)$ as given by the searching procedure. The final integration was stopped automatically at the point at which the first signs of divergence in the solutions appeared.

The location of point *a* and the value of Δ for the first stage of approximation were chosen arbitrarily, and T_c was taken to be 200000° K in all calculations.

IV. RESULTS AND DISCUSSION

Calculations were carried out for several values of each of the various parameters. In particular, the ranges of L and M appropriate to cepheids of both populations were

partially covered, and calculations for several values of R, for each L and M, were carried out.

We shall here present detailed numerical results only for certain selected models which are of greatest interest or which exhibit features common to most of the models. The behavior of models for which detailed results are not given will be summarized in qualitative statements.

All the discussion in this section is to be understood to apply only within the framework of the particular method of mathematical approximation that has been used for the treatment of the non-adiabatic problem (cf. Sec. I and footnotes at end of Sec. V).

The discussion in this section will be limited to the models for population I cepheids, because certain difficulties were encountered in the application of the helium-ionization theory to the population II cepheids; these difficulties rendered the results for these stars largely inconclusive. The basic source of the difficulty is to be found in the low surface gravity of the population II cepheids (assuming $M = 1.25$); second helium ionization occurs at such a great geometrical depth in the envelopes that the relative pulsation amplitude is rather small in this region. This may also be seen from equations (8) and (11). The values of D are so small that z must be relatively large in the region of second

TABLE 1

PHYSICAL CHARACTERISTICS OF MODEL 1

$\log L$	3.13
$\log M$	0.73152
n	0.70
s	2.10
n_e	3.00
B	0.15
$\bar{\mu}$	0.69565
$\log K_{n_e}$	−13.42508
$\log R$	1.527
D	6.3892×10^5 ° K
Q_d	0.04
Π_d	3.3639
Ω	2.897206
Γ_1 (in eq. [13])	$\frac{5}{3}$

helium ionization (the temperature here is not very sensitive to the envelope model). Also the relatively great curvature in these regions and the absence of interiors invalidate the approximate method of treating the adiabatic problem (cf. the discussion following eq. [12]). This great curvature, moreover, renders the total heat-storage capacity of the layers above the level of second helium ionization relatively small (in other words, $\phi[z^*] = \phi^*$, where z^* is the level of 50 per cent He^+ ionization, is very small, cf. eq. [37] and Sec. IV, *d*). For other elements (first helium ionization and hydrogen ionization), the geometrical depth would be less, but the corresponding values of ϕ^* would be far too small for these ionizations to be directly effective.

As a basis for comparison of some of the theoretical results with observation, we shall adopt the following expression for the empirical period-luminosity (Π-L) relation for classical cepheids:

$$\log L = 1.05 \log \Pi_d + 2.60 \ . \tag{50}$$

Equation (50) was obtained from equation (12) of Sandage (1958).

a) Results for a Particular Model

In Table 1 are summarized the physical properties of the model which we may regard as the prototype of the models adopted here for the classical cepheids; we shall call this

"Model 1." The values of R and Π for this model are close to the empirical values (log $R = 1.513$, $\Pi_d = 3.20$; cf. eqs. [15*b*] and [50]) for a classical cepheid of this luminosity. Also the values of n and s are such that equation (1) provides an adequate approximation to tabulated opacities in the regions of greatest interest.

In Tables 2*A*, 2*B*, and 2*C* are presented the results of the calculations for Parts I, II, and III, respectively, for Model 1, as functions of temperature T. Note that Part I does not involve either R or Q. The notation and formulae used have been explained in Sections II and III, *a;* however, the following comments should be made: (1) In Table 2*A*, Θ_T was computed from the formula

$$\Theta_T = \frac{(\Gamma_3 - 1)(1.5 + 125.3\theta) - 1}{125.3\theta}, \tag{51}$$

which can be obtained from equation (32). (2) In the tenth and eleventh columns of Table 2*C*, $|H_\kappa|$ and θ_H represent, respectively, the (normalized) semiamplitude of the relative flux variation and its phase relative to minimum radius; i.e.,

$$-H_\kappa = |H_\kappa| \exp(i\theta_H) . \tag{52}$$

Thus a negative value of θ_H ($> -\pi$) means that the relative flux variation reaches maximum *after* minimum radius; negative values of θ_H will be referred to as "phase lags"; positive values as "phase leads."

Some of the entries in Tables 2*A*, 2*B*, and 2*C* have been displayed in Figures 1, 2, and

TABLE 2A*

RESULTS OF PART I FOR MODEL 1

T(° K) $\times 10^{-3}$	η	$\Gamma_3 - 1$	$1/(\Gamma_2 - 1)$	$\frac{3}{2}\Theta_T$
0	0	0.666667	1.500000	1.000000
10		.666667	1.500000	1.000000
20	1.22415 (−7)	.666663	1.500009	0.999994
25	4.83471 (−5)	.665721	1.502211	0.998497
30	2.46846 (−3)	.634547	1.579295	0.948387
32	8.29674 (−3)	.580718	1.732462	0.861278
34	2.37779 (−2)	.488893	2.072606	0.711806
36	5.88937 (−2)	.381935	2.676968	0.536384
37	8.78403 (−2)	.334686	3.067999	0.458268
38	0.126340	.295839	3.483988	0.393555
40	0.233849	.245604	4.220339	0.308402
42	0.373583	.227032	4.580303	0.274765
44	0 521922	.232679	4.474242	0.280988
46	0.654125	.257664	4.037361	0.319468
48	0.757560	.298045	3.477446	0.384632
50	0.832027	.350230	2.951176	0.468977
52	0.883298	.406715	2.528984	0.561914
54	0.917979	.461194	2.218929	0.652262
56	0.941416	.508851	2.001621	0.731791
58	0 957392	.547606	1.852457	0.796806
60	0.968433	.577586	1.750580	0.847338
65	0.983890	.623236	1.613849	0.924796
70	0.990936	.644380	1.556810	0.961012
80	0.996393	.659507	1.518017	0.987220
100	0.998957	.665271	1.503549	0.997409
120	0.999521	.666203	1.501197	0.999107
140	0.999715	0.666457	1.500551	0.999580

*The numbers in parentheses are the powers of 10 by which the corresponding entries must be multiplied.

3. Figure 1 shows the runs of the quasi-adiabatic flux variation, $\mathfrak{H}_{1,a}$ (*solid curve*), and the phase, θ_H (*dashed curve*), of $-H_\kappa$, with T over a range which includes the region of second helium ionization. The dash-dot curve, labeled $\tilde{\mathfrak{H}}_{1,a}$, represents the curve that would have been obtained for $\mathfrak{H}_{1,a}$ if Γ_3 had been held constant and equal to $\frac{5}{3}$ (cf. eq. [35]), i.e., if second helium ionization had not been taken into account or if B had been set equal to zero. The large and abrupt decrease toward the surface in the $\mathfrak{H}_{1,a}$-curve shown in Figure 1 is brought about by the sudden increase in the heat-storage capacity of the stellar material in the region of second helium ionization (i.e., by the abrupt diminution in the values of $\Gamma_3 - 1$; cf. Table 2*A*). This abrupt decrease in the $\mathfrak{H}_{1,a}$-curve is

TABLE 2B*

RESULTS OF PART II FOR MODEL 1

T(° K) $\times 10^{-3}$	z	x	y	y'	ρ_1	$\mathfrak{H}_{1,a}$	$\mathfrak{H}'_{1,a}$	$\phi(z)$
0.....	0	1.00000	1.00000	4.0363	7.0363	+19.698	+ 98.256	0
10.....	1.5651 (−2)	0.98459	0.93923	3.8517	6.6100	+18.224	+ 91.912	1.8408 (−4)
20.....	3.1303 (−2)	0.96965	0.88297	3.6796	6.2168	+16.894	+ 86.836	5.5975 (−3)
25.....	3.9129 (−2)	0.96234	0.85640	3.5979	6.0316	+16.117	+ 173.74	1.6661 (−2)
30.....	4.6954 (−2)	0.95515	0.83081	3.5189	5.8535	+11.450	+1541.4	4.0879 (−2)
32.....	5.0085 (−2)	0.95230	0.82083	3.4881	5.7842	+ 5.6871	+2416.0	5.7235 (−2)
34.....	5.3215 (−2)	0.94947	0.81100	3.4576	5.7159	− 1.0387	+2055.0	8.1219 (−2)
36.....	5.6345 (−2)	0.94666	0.80131	3.4276	5.6487	− 4.7724	+ 550.62	0.11951
37.....	5.7910 (−2)	0.94526	0.79652	3.4127	5.6155	− 5.0703	− 89.144	0.14750
38.....	5.9475 (−2)	0.94386	0.79177	3.3979	5.5825	− 4.6328	− 499.95	0.18381
40.....	6.2606 (−2)	0.94108	0.78236	3.3687	5.5173	− 2.6915	− 819.77	0.28828
42.....	6.5736 (−2)	0.93832	0.77309	3.3398	5.4531	− 0.28229	− 918.10	0.44023
44.....	6.8866 (−2)	0.93557	0.76395	3.3113	5.3898	+ 2.3892	−1032.2	0.63158
46.....	7.1997 (−2)	0.93284	0.75494	3.2832	5.3275	+ 5.3624	−1134.0	0.84285
48.....	7.5127 (−2)	0.93012	0.74606	3.2555	5.2662	+ 8.4495	−1110.6	1.0559
50.....	7.8257 (−2)	0.92742	0.73731	3.2281	5.2057	+11.205	− 900.83	1.2618
52.....	8.1388 (−2)	0.92474	0.72868	3.2010	5.1461	+13.187	− 565.61	1.4597
54.....	8.4518 (−2)	0.92207	0.72017	3.1743	5.0874	+14.241	− 235.47	1.6536
56.....	8.7648 (−2)	0.91942	0.71178	3.1479	5.0296	+14.531	− 2.2411	1.8488
58.....	9.0778 (−2)	0.91678	0.70351	3.1219	4.9726	+14.353	+ 120.66	2.0505
60.....	9.3909 (−2)	0.91415	0.69536	3.0962	4.9165	+13.966	+ 164.94	2.2635
65.....	0.10173	0.90766	0.67546	3.0334	4.7797	+12.919	+ 143.25	2.8721
70.....	0.10956	0.90126	0.65623	2.9725	4.6477	+12.141	+ 102.56	3.6313
80.....	0.12521	0.88872	0.61970	2.8562	4.3975	+11.115	+ 68.605	5.7877
100.....	0.15651	0.86467	0.55358	2.6438	3.9468	+ 9.6773	+ 54.364	13.967
120.....	0.18782	0.84188	0.49551	2.4550	3.5533	+ 8.5094	+ 48.419	30.176
140.....	0.21912	0.82026	0.44428	2.2864	3.2083	+ 7.5148	+ 43.694	58.507

* The numbers in parentheses are the powers of 10 by which the corresponding entries must be multiplied.

seen to induce a large phase lag in the surface flux variation, amounting, in this case, to $\theta_H(0) = -45°.3$. Note also that the value of $\phi(z)$ (cf. eq. [37]) for this model is near unity in the region in which the abrupt drop in $\mathfrak{H}_{1,a}$ occurs (and therefore also in the region of second helium ionization). The significance of this last result for the stability problem has been discussed in N-A I and in Papers IV and V and will be discussed further in Sections IV, *b* and *d* of this paper.

The steep rise to relatively large values in the $\mathfrak{H}_{1,a}$-curve exterior to the region of second helium ionization is probably unrealistic, as first helium ionization and hydrogen ionization (which have been neglected here) would probably have prevented this increase from being so abrupt or pronounced. Since, as is seen from Table 2*A*, the material is convectively unstable in the region of second helium ionization, the variations in

TABLE 2C*

RESULTS OF PART III FOR MODEL 1

$T(^\circ K)\times10^{-3}$	v_1	v_2	V_1	$V_2=H_2$	H_1	dH_1/dz	$\lvert H_K\rvert$	θ_H (degrees)	I_1, (0, z)
0.....	−2.4450	−0.79115	−14.915	−4.8260	4.7740	0	6.7884	−45.310	0
10.....	−2.2374	−0.79138	−13.449	−4.8286	4.7749	+ 0.28096	6.7908	−45.320	− 3.9571 (−3)
20.....	−2.0444	−0.79778	−12.092	−4.8980	4.8012	+ 4.2628	6.8587	−45.572	− 0.11480
25.....	−1.9443	−0.81023	−11.262	−5.0323	4.8554	+ 10.270	6.9928	−46.025	− 0.33576
30.....	−1.6650	−0.83577	− 6.4733	−5.3022	4.9770	+ 22.448	7.2722	−46.812	− 0.80819
32.....	−1.3152	−0.85079	− 0.62593	−5.4517	5.0612	+ 32.200	7.4389	−47.127	− 1.1064
34.....	−0.75320	−0.86815	+ 6.2258	−5.6022	5.1870	+ 50.118	7.6348	−47.204	− 1.4927
36.....	−0.11403	−0.88574	+10.165	−5.6965	5.3921	+ 84.473	7.8438	−46.573	− 1.9940
37.....	+0.16779	−0.89317	+10.614	−5.6903	5.5440	+110.80	7.9445	−45.746	− 2.2991
38.....	+0.40211	−0.89844	+10.375	−5.6251	5.7425	+143.90	8.0385	−44.408	− 2.6477
40.....	+0.72216	−0.89752	+ 9.0072	−5.2494	6.3157	+224.12	8.2125	−39.732	− 3.4934
42.....	+0.88191	−0.87268	+ 7.4200	−4.4920	7.1377	+296.47	8.4366	−32.184	− 4.5464
44.....	+0.93013	−0.81730	+ 5.7370	−3.4246	8.1262	+326.28	8.8183	−22.852	− 5.7688
46.....	+0.89408	−0.73264	+ 3.7648	−2.2412	9.1273	+306.27	9.3984	−13.796	− 7.0754
48.....	+0.78847	−0.62726	+ 1.5634	−1.1408	10.013	+256.87	10.078	− 6.500	− 8.3714
50.....	+0.63199	−0.51275	− 0.47512	−0.24432	10.729	+201.34	10.732	− 1.304	− 9.5819
52.....	+0.45308	−0.39965	− 1.9065	+0.41203	11.280	+151.94	11.288	+ 2.092	−10.657
54.....	+0.28240	−0.29547	− 2.5509	+0.84500	11.690	+111.48	11.721	+ 4.134	−11.565
56.....	+0.14181	−0.20450	− 2.5446	+1.0936	11.986	+ 78.746	12.036	+ 5.213	−12.290
58.....	+3.9756 (−2)	−0.12849	− 2.1639	+1.2009	12.189	+ 51.738	12.248	+ 5.627	−12.826
60.....	−2.5888 (−2)	−6.7411 (−2)	− 1.6512	+1.2058	12.314	+ 28.920	12.373	+ 5.593	−13.174
65.....	−8.0642 (−2)	+2.8223 (−2)	− 0.56064	+0.96823	12.358	− 14.865	12.396	+ 4.480	−13.299
70.....	−6.4962 (−2)	+6.4674 (−2)	− 1.8439 (−2)	+0.62045	12.123	− 42.877	12.139	+ 2.930	−12.593
80.....	−1.6638 (−2)	+5.7620 (−2)	+ 0.14596	+0.13788	11.261	− 60.002	11.262	+ 0.702	−10.048
100.....	+2.6084 (−4)	+1.8270 (−2)	− 6.1877 (−3)	+2.0358 (−2)	9.6711	− 41.201	9.6711	+ 0.121	− 5.6397
120.....	−9.3138 (−5)	+8.1731 (−3)	− 2.6329 (−3)	+1.4977 (−2)	8.5067	− 34.290	8.5068	+ 0.101	− 2.7314
140.....	−2.3961 (−5)	+4.2020 (−3)	− 2.9951 (−3)	+7.3982 (−3)	7.5118	− 29.419	7.5118	+ 0.056	− 0.48943

* The numbers in parentheses are the powers of 10 by which the corresponding entries must be multiplied.

convective flux, if taken into account, might also have tended to depress the $\mathfrak{H}_{1,a}$-curve in this region. The effects of this abrupt rise in the $\mathfrak{H}_{1,a}$-curve on the surface flux variations and on the stability problem turned out to be more serious than had been anticipated in the planning stages of the investigation and will be discussed in more detail later in this section and in Sections IV, *b* and *c*.

Convective instability in the region of second helium ionization occurred in all models having $B = 0.15$ or 0.25 but did not occur for $B = 0.05$. The critical value of B for which convective instability occurs therefore probably lies between 0.05 and 0.10.

The effect of this convective instability on the structure of the envelopes has not been analyzed in detail. Rough calculations suggest, however, that this effect will be small for the cepheids.

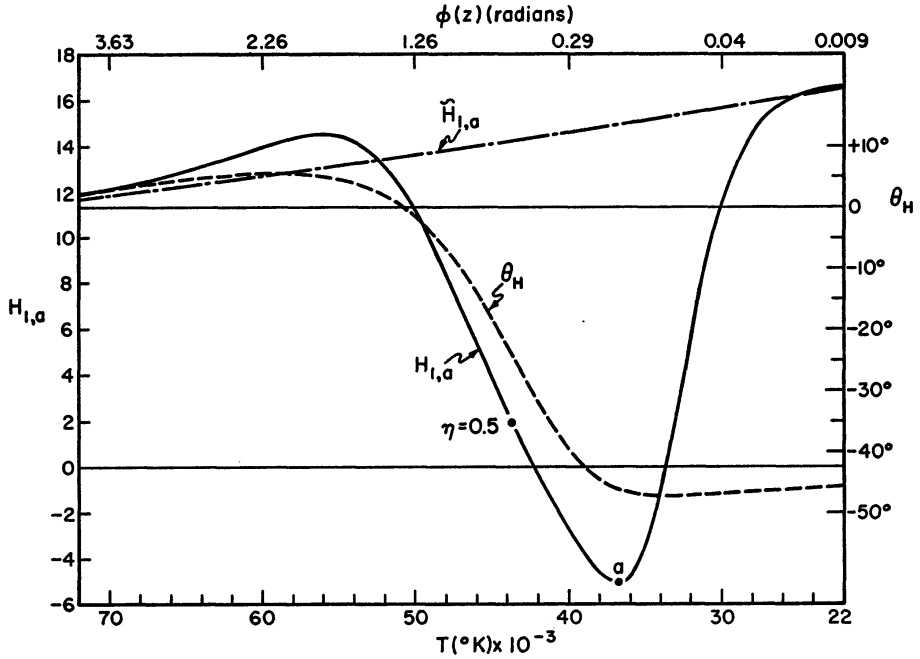

FIG. 1.—Quasi-adiabatic flux variation and phase of non-adiabatic flux variation for Model 1. The solid curve (*scale at left*) shows the actual (normalized) quasi-adiabatic flux variation, while the dash-dot curve shows the quasi-adiabatic flux variation which would have been obtained if second helium ionization had not been taken into account or if B (helium/hydrogen ratio) had been set equal to zero. The dashed curve (*scale at right*) shows the phases (relative to minimum radius) of the maxima of the non-adiabatic flux variations. Values of the phase-lag function $\phi(z)$ (cf. eqs. [37] and [33]) are given at the top of the figure. The level of 50 per cent ionization of He^+ is also indicated on the figure.

Figure 2 shows $\mathfrak{H}_{1,a}$ as a function of ϕ (cf. eq. [37]) for Model 1.

In Figure 3 the runs of $-V_\kappa(z)$ (*dashed curve*) and $-H_\kappa(z)$ (*solid curve*) as functions of z (or T) are presented in a polar plot. The small numbers beside the plotted points denote the corresponding values of T. On this type of diagram, y (relative pulsation amplitude) and $\mathfrak{H}_{1,a}$, if positive, would be represented by vectors lying along the positive real axis. The abrupt turn to the left in the $-V_\kappa(z)$-curve corresponds to the minimum of the $\mathfrak{H}_{1,a}$-curve (point *a* in Figs. 1 and 2), and the turn to the right corresponds, approximately, to the maximum of the $\mathfrak{H}_{1,a}$-curve. The upward turn in the $-\mathfrak{H}_\kappa(z)$-curve for $T \lesssim 36000°$ K is caused by the abrupt rise toward the surface in the $\mathfrak{H}_{1,a}$-curve exterior to the region of second helium ionization. If $\mathfrak{H}_{1,a}$ had remained approximately constant exterior to point *a*, this upward turn in the $-H_\kappa(z)$-curve would not have occurred, and $-H_\kappa(0)$, the surface value of $-H_\kappa(z)$, would have had both a larger amplitude and a larger

phase lag than is actually the case in Figure 3. The encircled dot in Figure 3 shows the value that $-H_\kappa(0)$ would have had if $\mathfrak{H}_{1,\,a}$ had remained constant and equal to its minimum value at all points exterior to point a in Figures 1 and 2. The co-ordinates of the encircled point in Figure 3 are given in parentheses in Table 3. These values were computed from the analytic theory (cf. Sec. II, *d*).

It is seen from the negative values of I_1 (0, z) in Table 2*C* that the envelope is exerting a destabilizing influence on the pulsations; this again is a consequence of the abrupt

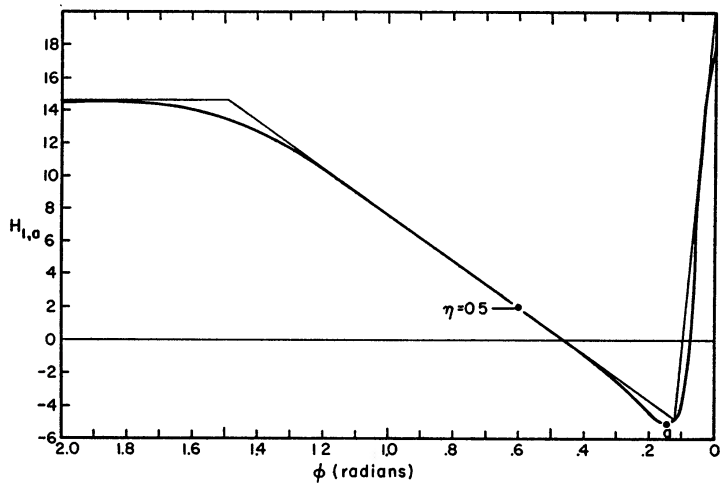

FIG. 2.—$\mathfrak{H}_{1,a}$ as a function of ϕ for Model 1. The point corresponding to 50 per cent ionization of He^+ is shown in the figure. The three light straight lines represent the schematized $\mathfrak{H}_{1,a}$-curve that was adopted in the three-zone model used for the calculations described in Section III, *b*, with the analytic theory (cf. Sec. II, *d*).

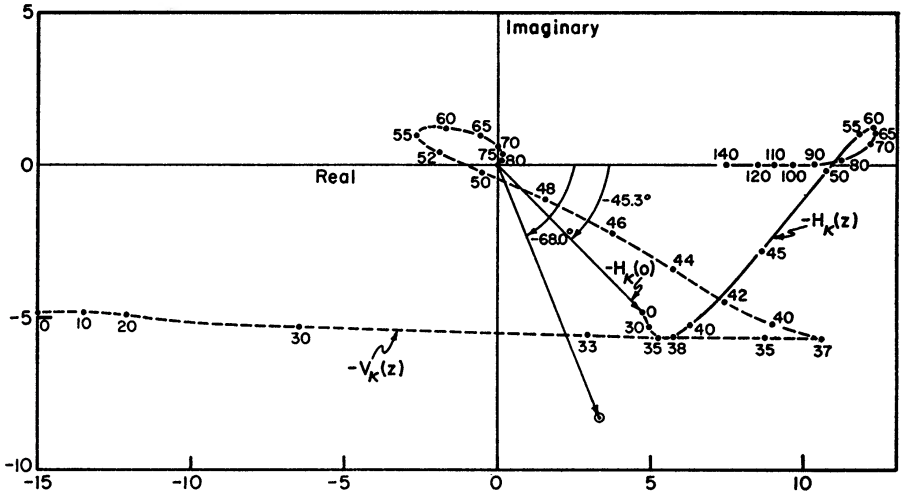

FIG. 3.—Polar plot of non-adiabatic flux variation as a function of depth for Model 1. The solid curve represents the non-adiabatic flux variation, $-H_\kappa(z)$, and the dashed curve represents the non-adiabatic contribution, $-V_\kappa(z)$, to the flux variation. All phases are relative to minimum radius. The numbers beside the plotted points denote the corresponding temperatures. The relative pulsation amplitude, y_κ (real and positive here), lies along the positive real axis. Arrows represent the surface flux variations, $-H_\kappa(0)$. The encircled dot shows the location that $-H_\kappa(0)$ would have had if the $\mathfrak{H}_{1,a}$-curve had remained constant and equal to its minimum value at all points exterior to the minimum (point *a* in Figs. 1 and 2).

decrease outward in the $\mathfrak{H}_{1,\,a}$-curve in the region of second helium ionization. The direct destabilizing influence produced by the action of second helium ionization can be appreciated more fully if the values of $I_1\,(0, z)$ in the region in which this function attains minimum (say at z_1) are examined; z_1 is also the point at which H_1 attains maximum. The increase in the value of $I_1\,(0, z)$ for $z > z_1$ is caused by the decrease in the H_1-curve toward the stellar center; this decrease gives a positive (or stabilizing) contribution to $I_1\,(0, z)$ (cf. eq. [38*a*]). For values of z much greater than z_1, however, the positive contribution to $I_1\,(0, z)$ becomes relatively insensitive to the effects of second helium ionization, for two reasons. First, $\Gamma_3 \rightarrow \frac{5}{3}$ and $\mathfrak{H}_{1,\,a}\,(z) \rightarrow \tilde{\mathfrak{H}}_{1,\,a}$ (cf. Fig. 1). Second, $\phi(z)$ becomes much greater than unity; this has the consequence that $|V_\kappa\,(z)| \ll |\mathfrak{H}_{1,\,a}\,(z)|$ or that the quasi-adiabatic flux variations begin to provide a good approximation to the actual, non-adiabatic flux variations. (This was shown in N-AI; the result can also be shown to follow from the Woltjer v-equations. The numerical work provides still further confirmation of this, as may be seen from the entries in Table 2*C*). Thus the *non-adiabatic* effects produced by second helium ionization also become insignificant. We shall arbitrarily adopt $I_1\,(0, z_1)$ as an approximate measure of the direct destabilizing effects produced by the action of second helium ionization in the envelopes. The stability problem will be discussed further in Section IV, *c*.

b) Dependence of Surface Flux Variations on R, B, and M

We now consider the dependence of $-H_\kappa(0)$, the surface value of $-H_\kappa(z)$, on radius R, helium abundance B, and mass M (or luminosity L). In Table 3 are presented values of $H_1\,(0)$, $H_2\,(0)$, $|H_\kappa(0)|$, and $\theta_H\,(0)$, with R as the independent variable, for three values of B and two values of $\log L$, for the case $n = 0.70$, $s = 2.10$, and $Q_d = 0.04$. These results are also presented in a polar plot in Figure 4. The solid curves are for $\log L = 3.13$, $\log M = 0.73152$, and the dashed curve is for $\log L = 4.13$, $\log M = 1.03552$. The numbers beside the plotted points denote the corresponding values of $\log R$.

It is seen from Table 3 or Figure 4 that, for $B = 0.15$ (both values of $\log L$) and 0.25, the phase lags in the surface flux variations are generally in the same quadrant as the observed phase lags (say 70°–90°) of classical cepheids, for reasonable values of R. For orientation, the empirical values (cf. eqs. [15*b*] and [50]) are $\log R = 1.513$ for $\log L = 3.13$ and $\log R = 2.248$ for $\log L = 4.13$. The computed phase lags are, however (in particular for $B = 0.15$), a little smaller than the observed ones; a possible reason for this will be given later in this section. For $B = 0.05$, the phase lags are seen to amount to only a few degrees and in some cases to be negative. While the v-equations were not integrated explicitly for the case $B = 0$, it may be inferred from extrapolation of the results given in Figure 4 or from analytic considerations that, in this case, phase leads in the surface flux variations, rather than phase lags, would have resulted. As was pointed out in Section IV, *a*, this case is characterized by a steady rise in the $\mathfrak{H}_{1,\,a}$-curve toward the surface (cf. Fig. 1).

In order to effect a rough comparison of the amplitudes, $|H_\kappa(0)|$, of the surface flux variations shown in Figure 4 with observations, we proceed as follows. We denote by $\Delta M_{\rm bol}$ the total range in the (bolometric) magnitude of the light-variation, i.e.,

$$\frac{L_{\max}}{L_{\min}} = 10^{0.4\,\Delta M_{\rm bol}}. \tag{53}$$

However, $|H_\kappa(0)|$ is the normalized *semiamplitude* of the surface luminosity variation, i.e.,

$$|\,H_\kappa\,(0)\,| \equiv \frac{\Delta L}{\eta_0 L}, \tag{54}$$

where ΔL and L are, respectively, the semiamplitude of the luminosity variation and the mean luminosity itself, and $\eta_0 = |\delta R/R|$ is the surface value of the relative pulsation semiamplitude. (We assume sinusoidal light-variations, as we must in a linear theory.) We then obtain

$$\Delta M_{\rm bol} = 2.5 \log_{10} \frac{1 + \eta_0 |H_\kappa(0)|}{1 - \eta_0 |H_\kappa(0)|}. \tag{55}$$

Some values of $\Delta M_{\rm bol}$ are presented in Table 4, with $|H_\kappa(0)|$ as the independent variable, for three values of η_0.

By comparing the entries given in Table 3 for $|H_\kappa(0)|$—say for $B = 0.15$, $\log L = 3.13$—with those in Table 4 (for $\eta_0 = 0.05$, a value which seems to be consistent with observations of classical cepheids), it is seen that the computed values of $\Delta M_{\rm bol}$, for reasonable values of R, are comparable to, but somewhat smaller than, the values of $\Delta M_{\rm bol}$ based on observations for most cepheids. (The photographic amplitudes for the classical cepheids generally range between about $0^m.5$ and $2^m.0$; for cepheids with periods less than 10 days, the range is between $0^m.5$ and $1^m.5$, with $1^m.0$ being perhaps the most

TABLE 3

PHASE AND AMPLITUDE OF SURFACE FLUX VARIATIONS AS FUNCTIONS OF RADIUS AND HELIUM ABUNDANCE

($n=0.70$, $s=2.10$, $Q_d=0.04$)

B	$\log R$	$H_1(0)$	$H_2(0)$	$\lvert H_\kappa(0)\rvert$	$\theta_H(0)$ (degrees)
	$\log L=3.13$, $\log M=0.73152$				
0.05	1.477	+7.756	−1.478	7.896	−10.79
	1.527	+6.849	−0.599	6.875	− 5.00
	1.577	+6.217	+0.484	6.236	+ 4.45
	1.627	+5.926	+1.681	6.159	+15.84
.15	1.477	+6.573	−5.331	8.463	−39.04
	1.527	+4.774	−4.826	6.788	−45.31
		(+3. 34)	(−8.26)	(8.910)	(−68.0)
	1.577	+3.170	−3.904	5.029	−50.92
	1.627	+1.900	−2.637	3.251	−54.23
	1.677	+1.054	−1.143	1.555	−47.31
	1.777	+0.726	+2.002	2.130	+70.08
		(−2.0±1.0)	(−4.3±1.0)	(4.7±1.4)	(−115±20)
.25	1.627	+1.105	−4.760	4.887	−76.94
	1.677	−0.202	−3.280	3.286	−93.52
	1.727	−1.002	−1.622	1.907	−121.72
	$\log L=4.13$, $\log M=1.03552$				
0.15	2.263	+3.118	−2.570	4.040	−39.49
	2.313	+2.105	−2.028	2.933	−43.94
	2.363	+1.299	−1.336	1.863	−45.80
	2.413	+0.726	−0.559	0.916	−37.62
	2.463	+0.383	+0.233	0.448	+31.32
	2.613	+0.434	+2.184	2.227	+78.76

typical value [cf. Ledoux and Walraven 1958, p. 373]. The bolometric amplitudes are not likely to differ greatly from the photographic.) For example, for $B = 0.15$, $\log L = 3.13$, $\log R = 1.527$, and $\eta_0 = 0.05$, we have $\Delta M_{bol} = 0^m.77$.

The amplitudes of the surface flux variations are generally smaller for $\log L = 4.13$ than for $\log L = 3.13$ ($B = 0.15$). This can be attributed (as in the case of the population II cepheid models) to the relatively small surface gravities of models with $\log L = 4.13$, with reasonable radii (or to the small values of D; cf. eqs. [8] and [11]), as compared with those for $\log L = 3.13$. The values of z (i.e., geometrical depth) at the level of second helium ionization are greater for $\log L = 4.13$ than for $\log L = 3.13$, so that the relative

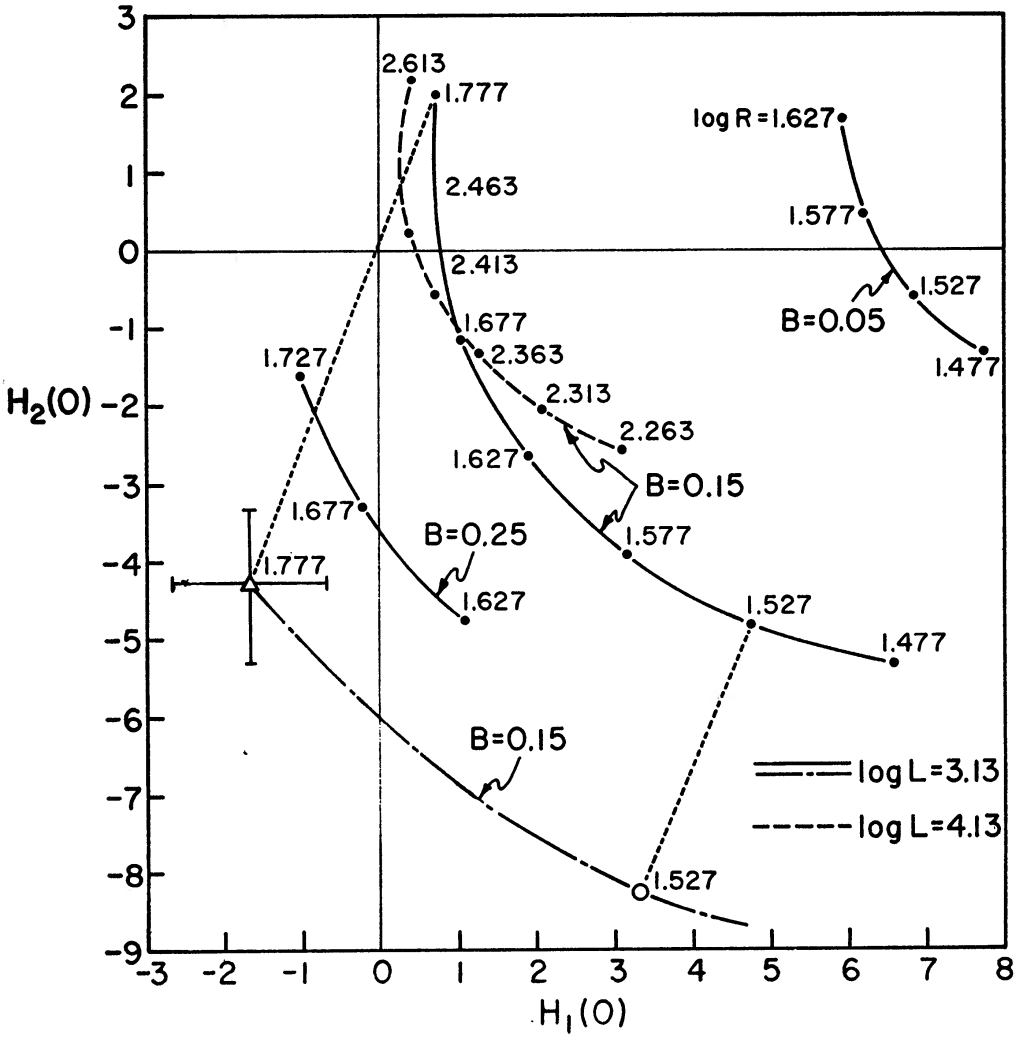

FIG. 4.—Surface flux variations for the case $n = 0.70$, $s = 2.10$, $Q = 0.04$ day. Here $H_1(0)$ and $H_2(0)$ denote, respectively, the real and imaginary parts of $-H_\kappa(0)$, the (normalized) surface flux variation. The phases are relative to minimum radius. Each curve shows the variation of $-H_\kappa(0)$ with radius, R, for the particular value of helium abundance, B, indicated alongside the appropriate curve. Solid lines are for $\log L = 3.13$, $\log M = 0.73152$ (solar units); dashed line for $\log L = 4.13$, $\log M = 1.03552$. The numbers beside the plotted points denote the corresponding values of $\log R$ (solar units). The empirical values (cf. eqs. [15b] and [50]) are $\log R = 1.513$ for $\log L = 3.13$, $\log R = 2.248$ for $\log L = 4.13$. The dash-dot curve shows the approximate location which the curve for $\log L = 3.13$, $B = 0.15$, would have had if the $\mathfrak{P}_{1,a}$-curve had remained constant and equal to its minimum value at all points exterior to the minimum (point a in Figs. 1 and 2). See text for further explanation of this curve.

pulsation amplitudes (and hence the quasi-adiabatic flux variations) are smaller at this level in the former case than in the latter. Because of the relatively large values of z at the level of second helium ionization for $\log L = 4.13$, the approximate method of treating the adiabatic problem renders these results less reliable than those for $\log L = 3.13$ (cf. the discussion following eq. [12] and Sec. IV, *c*).

We now consider the possible effects on the surface flux variations of some of the approximations made in computing the $\mathfrak{H}_{1,a}$-curve. It should be noted, first, that the primary factor determining the character of the surface flux variations is the behavior of those portions of the $\mathfrak{H}_{1,a}$-curve that lie in the region with $\phi(z) \approx 1$ (this is the "critical region" discussed by Eddington 1927 and in N-AI, Sec. III). In regions with $\phi(z) \gg 1$, the non-adiabatic effects are insignificant (cf. last paragraph in Sec. IV, *a*), whereas, in regions with $\phi(z) \ll 1$, the $H_\kappa(z)$ vector is effectively "frozen in" (this may be seen from eq. [30] or from the entries in Table 2*c*). The large phase lags in the surface

TABLE 4

RELATION OF ΔM_{bol} TO $|H_\kappa(0)|$

$\lvert H_\kappa(0)\rvert$	ΔM_{bol}		
	$\eta_0 = 0.04$	$\eta_0 = 0.05$	$\eta_0 = 0.10$
1	0.0869	0.109	0.218
2	0.172	0.218	0.440
3	0.262	0.328	0.672
4	0.350	0.440	0.920
5	0.440	0.555	1.193
6	0.532	0.672	1.505
7	0.625	0.794	1.883
8	0.720	0.920	2.386
9	0.818	1.053	3.197
10	0.920	1.193	.....
12	1.136	1.505	.....
14	1.374	1.883	.....
16	1.646	2.386	.....
18	1.971	3.197	.....
20	2.386	.....	.....

flux variations obtained here (for reasonable radii) are due not only to the abrupt outward decrease itself in the $\mathfrak{H}_{1,a}$-curve in the region of second helium ionization (first helium ionization and hydrogen ionization would have produced qualitatively similar decreases) but also to the fact that the decrease occurs, for second helium ionization, just in the critical region (cf. Figs. 1 and 2). It was because first helium ionization and hydrogen ionization both occur in regions with $\phi(z) \ll 1$ (for radii in the cepheid domain) that it was felt safe to neglect these ionizations in this investigation.

However, these ionizations, if included, would have acted indirectly by decreasing the extent and steepness of the increase toward the surface in the $\mathfrak{H}_{1,a}$-curve exterior to the region of second helium ionization. The effect of removing this increase completely for the model with $\log L = 3.13$, $B = 0.15$, and $\log R = 1.527$ is shown by the location of the encircled dot in Figure 4. The location of this point (whose co-ordinates are given in parentheses in Table 3) was computed from the analytic theory (cf. Sec. II, *d*) by assuming $\mathfrak{H}_{1,a}$ to remain constant and equal to its minimum value at all points exterior to the minimum (point *a* in Figs. 1 and 2). It is seen from the extent of the shift that the effects of the steep rise in the $\mathfrak{H}_{1,a}$-curve are not negligible. The reason for this is that the magnitude of the slope of the $\mathfrak{H}_{1,a}$-curve (with respect to ϕ; cf. Fig. 2) is very large

at points exterior to point a, and the values of ϕ in the region of the rapid increase are not sufficiently small for the "freezing-in" of $H_\kappa(z)$ to be effective.

In general, the result of completely removing the abrupt increase in the $\mathfrak{H}_{1,\,a}$-curves would be to cause all points in Figure 4 to be moved downward and to the left by amounts which increase with increasing R (for given B). Because the calculations with the analytic theory are quite laborious even for a three-zone model, the shift was accurately computed only for the one case (*open circle*) mentioned in the preceding paragraph. The shift for the model with $\log L = 3.13$, $B = 0.15$, and $\log R = 1.777$ was obtained from an estimate based on the analytic theory, and the new location is shown by the triangle in Figure 4 (the co-ordinates of this point are also given in parentheses in Table 3). The estimate of the location of this point is inaccurate by, at most, plus or minus one unit (the possible error is shown by bars through the point). These two shifted points have been connected by the dash-dot curve shown in the figure; this then represents approximately the curve which would have been obtained for the case $\log L = 3.13$, $B = 0.15$, if the increase in the $\mathfrak{H}_{1,\,a}$-curve exterior to point a in Figures 1 and 2 had been removed altogether.

It is clear that the shifted curve is in much better agreement with observations of classical cepheids than the original curve. The amplitude of the light-variations ranges between $0^m.52$ for $\log R = 1.777$ and $1^m.04$ for $\log R = 1.527$ (assuming $\eta_0 = 0.05$), while the phase lag ranges between 115° and 68°, for the same respective values of $\log R$. In addition, it is shown in Section IV, *c*, that maximum instability occurs, in the case of the original curve, for $\log R \approx 1.7$. While this value of $\log R$ would certainly have been altered somewhat if stability calculations had been carried out for the case of the shifted curve, it is clear that the phase lag corresponding to maximum instability would have been close to 90°, which is approximately the observed phase lag of most classical cepheids. The phase lag would not have been greatly different from 90°, in fact, if maximum instability had occurred for *any* value of $\log R$ between 1.527 and 1.777. If the shifted curve actually corresponded to classical cepheids, it would provide a natural explanation of the common tendency of the observed phase lags to cluster around 90°. While the shifted curve must obviously represent a gross oversimplification of the actual situation, it is probable that the results of the numerical calculations would have been considerably improved if those physical factors (in particular, first helium ionization and hydrogen ionization) which would depress the $\mathfrak{H}_{1,\,a}$-curve in the region exterior to the zone of second helium ionization had been taken into account.

Another approximation made in the computation of the $\mathfrak{H}_{1,\,a}$-curves is the simple form of the opacity law (cf. eq. [1]). The effect of the variation of the exponents n and s with depth has apparently been taken into account by Zhevakin (1959), and his $\mathfrak{H}_{1,\,a}$-curves do not differ significantly from those obtained in this investigation. The assumption of constancy of n and s has therefore evidently not introduced any very large errors into the present calculations.

c) Dependence of Pulsational Instability on R, B, and M

The question of the pulsational stability of the star can be answered, in principle, by determining the sign of $I_1(0, \infty)$ (cf. eqs. [38*a*], [38*d*]). If, as in the present case, interiors are not available, the best that one can do is to use the results of the integrations to evaluate the contribution to $I_1(0, \infty)$ from the envelopes alone and then to estimate in some way the contribution from the remainder of the star.

We shall set $z = z_1$ in equation (38*d*), where z_1 is the value of z for which $I_1(0, z)$ attains minimum. In accordance with the discussion in Section IV, *a*, $I_1(0, z_1)$ may be regarded as an approximate measure of the direct destabilzing influence produced by second helium ionization in the envelopes. These values of $I_1(0, z_1)$ are taken from the integrations and are given in Table 5, with R as the independent variable, for three values of B (0.05, 0.15, and 0.25) and two values of $\log L$ (3.13 and 4.13), for the case

$n = 0.70$, $s = 2.10$, and $Q_d = 0.04$. Here T_1 is the temperature at the point z_1. Values of $I_1(0, z_1)$ are also displayed in Figure 5 (*dashed curve*) for $\log L = 3.13$, $B = 0.15$.

We may obtain an estimate of the values of $I_1(z_1, \infty)$, the positive contribution to $I_1(0, \infty)$ from the regions interior to z_1, in the following way. Write

$$I_1(z_1, \infty) = I_1(z_1, z_2) + I_1(z_2, \infty), \tag{56}$$

where z_2 denotes the greatest depth to which any particular final integration was carried. Values of $I_1(z_1, z_2)$ are also available from the integrations. The value of $I_1(z_2, \infty)$ may be estimated by taking $\Theta_p = \frac{2}{3}$ in equation (38*a*) and integrating by parts, to obtain (neglecting the effects of nuclear energy production)

$$I_1(z_2, \infty) = \frac{2}{3}\left[(\rho_1 H_1)_{z_2} - (\rho_1 H_1)_{\infty} - \int_{z_2}^{\infty} H_1\left(-\frac{d\rho_1}{dz}\right) dz\right]. \tag{57}$$

For giant-star models, $(\rho_1 H_1)_\infty$ (i.e., the central value of $\rho_1 H_1$) is invariably much smaller than $(\rho_1 H_1)_{z_2}$ and so may be neglected. In addition, the integral in equation (57) will be some fraction of $(\rho_1 H_1)_{z_2}$, the value of this fraction depending on z_2. Thus we write equation (57) in the form

$$I_1(z_2, \infty) = \tfrac{2}{3}\alpha(z_2)(\rho_1 H_1)_{z_2}. \tag{58}$$

TABLE 5

RESULTS OF STABILITY CALCULATIONS

($n=0.70$, $s=2.10$, $Q_d=0.04$, $\alpha=\frac{1}{2}$)

B	$\log R$	T_1(° K) $\times 10^{-3}$	z_1	$-I_1(0, z_1)$	$I_1(z_1, \infty)$	$I_1(0, \infty)$
	$\log L=3.13$, $\log M=0.73152$					
0.05	1.477	61.0	0.10359	10.551	+20.083	+ 9.532
	1.527	60.5	.11528	10.991	+18.770	+ 7.771
	1.577	59.5	.12720	10.502	+17.285	+ 6.783
	1.627	58.5	.14030	8.924	+15.781	+ 6.857
.15	1.477	64.0	.08928	11.347	+22.007	+10.660
	1.527	63.0	09860	13.367	+20 911	+ 7.544
	1.577	62.0	.10888	14.773	+19.634	+ 4.861
	1.627	61.0	.12019	15.334	+18.244	+ 2.910
	1.677	60.0	.13265	14.924	+16.836	+ 1.912
	1.777	58.0	.16143	11.204	+13.888	+ 2.684
.25	1.627	62.0	.10623	15.484	+19.844	+ 4.360
	1.677	61.5	.11823	15.879	+18.671	+ 2.792
	1.727	60.0	0.12942	15.373	+17.239	+ 1.866
	$\log L=4.13$, $\log M=1.03552$					
0.15	2.263	54.0	0.22853	4.175	+ 6.951	+ 2.776
	2.313	53.5	.25404	4.349	+ 5.943	+ 1.594
	2.363	53.0	.28238	4.214	+ 5.079	+ 0.865
	2.413	52.5	.31384	3.787	+ 4.210	+ 0.423
	2.463	52.0	.34878	3.122	+ 3.417	+ 0.295
	2.613	51.0	0.48320	0.511	+ 0.702	+ 0.191

The values of z_2 are in all cases such that $\phi(z_2) \gg 1$, so that, for points interior to z_2, $|H_\kappa| \approx |\mathfrak{H}_{\kappa,\,a}|$ (cf. last paragraph in Sec. IV, *a*). Thus the behavior of $a(z_2)$ can be estimated by examining the quasi-adiabatic flux variations associated with models for which solutions of the adiabatic wave equation are available. In all cases ρ_1 and $\mathfrak{H}_{1,\,a}$ decrease monotonically toward the center for points interior to z_2. In such cases, $a(z_2)$ is a slowly varying function of z_2, and its value lies between zero and unity.

Zhevakin (1958) has discussed the dependence of the function $a(z_2)$, defined in equation (58), on z_2 and on the exponents n and s in the opacity law (cf. eq. [1]), for the quasi-adiabatic oscillations of several stellar models, assuming radiative transfer. (In Zhevakin's notation, our function a is denoted by z.) He has shown the following: (1) For giant-star models whose outer parts are in radiative equilibrium, $a(z_2)$ is practically independ-

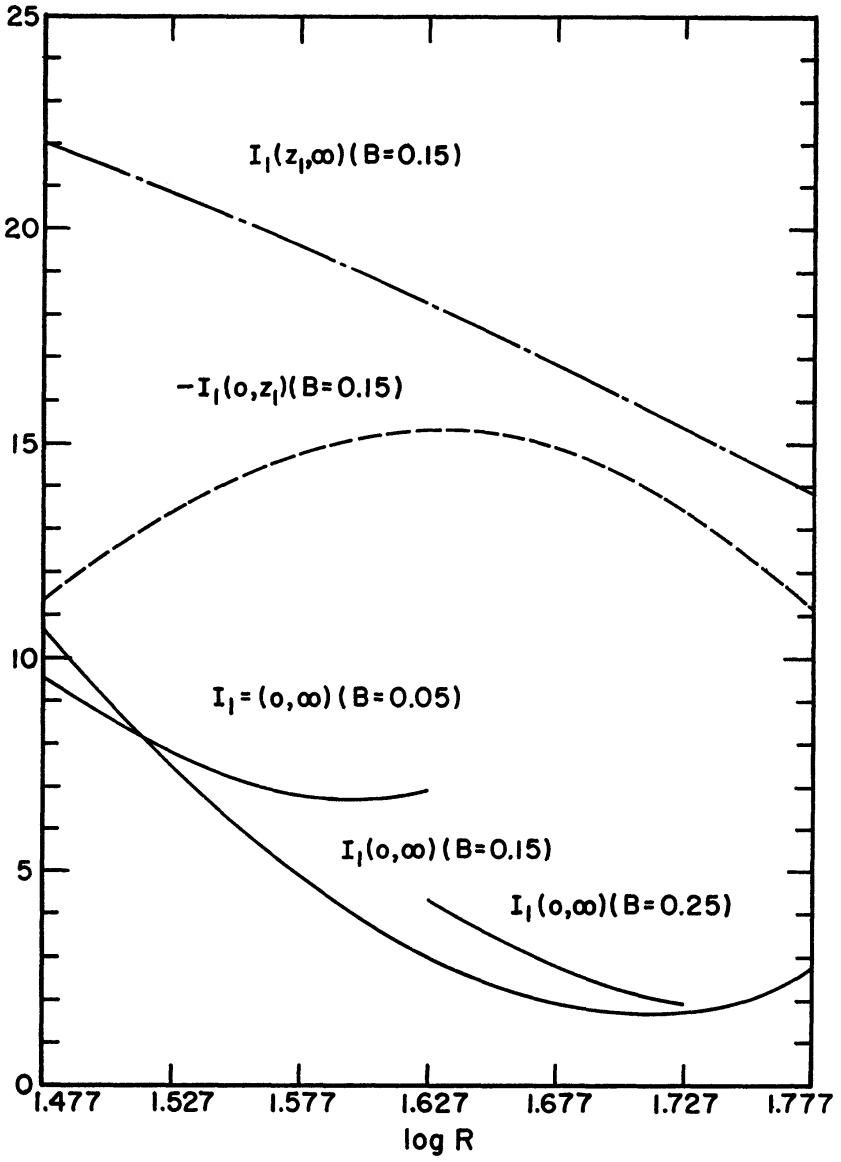

FIG. 5.—Stability integrals for log L = 3.13, log M = 0.73152 (solar units), n = 0.70, s = 2.10, Q_d = 0.04 (see text for explanation of symbols). The appropriate values of B (helium/hydrogen ratio) are indicated alongside the various curves. The radii are in solar units.

ent of z_2 for $z_2 < 1$ (corresponding to $x_2 > \frac{1}{2}$). (2) The value of a, for $z_2 < 1$, is very insensitive to the stellar model, in particular to the degree of mass concentration toward the center, and hence to the degree of "non-homologousness" (i.e., the rapidity of the rate of increase of ρ_1 toward the surface) of the pulsations. (3) For giant-star models with $0.5 < n < 1.5$, $1 < s < 5$ (the range of values of practical interest), equation (58) will be accurate to within better than 4 per cent for $z_2 < 1$ if a is assigned the value 0.535.

Equation (58) therefore evidently gives a good estimate of the value of $I_1(z_2, \infty)$, and the principal uncertainty lies in the values of $(\rho_1 H_1)_{z_2}$, which are taken from the integrations (cf. next two paragraphs). In computing $I_1(z_2, \infty)$, we shall assume that a is independent of z_2 and shall adopt the value $a = \frac{1}{2}$. Values of $I_1(z_1, \infty)$, computed in this way, are also presented in Table 5 and are plotted in Figure 5 for the case $\log L = 3.13$, $B = 0.15$ (*dash-dot curve*). In this table also are given the corresponding values of $I_1(0, \infty)$, computed from equation (38*d*), with $z = z_1$. Values of $I_1(0, \infty)$ are plotted in Figure 5 for the case $\log L = 3.13$, with three values of B (0.05, 0.15, and 0.25, *solid curves*).

We note that $I_1(0, \infty)$ is positive in all cases shown in Table 5, thus indicating stability against pulsations. It is seen, however, that the values of $|I_1(0, z_1)|$ are roughly comparable to the corresponding values of $I_1(z_1, \infty)$; this means that the destabilizing effects of second helium ionization in the envelopes are roughly comparable in magnitude to the stabilizing effects of the interior regions. Consequently, any error in either or both of $|I_1(0, z_1)|$ and $I_1(z_1, \infty)$ will be greatly magnified in $I_1(0, \infty)$, which is the *difference* between these two quantities.

The uncertainties involved in $I_1(z_1, \infty)$ are more serious than for $I_1(0, z_1)$ (for given ionizing constituents), because most of the contribution to $I_1(z_1, \infty)$ comes from regions with relatively large values of z; and, as is pointed out elsewhere (cf. the discussion following eq. [12] and Sec. IV, *e*), the approximate method of treating the adiabatic problem is subject to considerable error in such regions. If, for example, all values of $I_1(z_1, \infty)$ in Table 5 were actually too large by, say, 50 per cent (a not unreasonable value), $I_1(0, \infty)$ would have been negative (indicating pulsational instability) for most of the values of $\log R$ in Table 5, for $B \geq 0.15$, and the stability situation would have been marginal for $B = 0.05$. (Note that, because of the relatively high accuracy of eq. [58], uncertainties in $I_1[z_1, \infty]$ arise only *indirectly* from the absence of interiors.) In view of these considerations, it does not seem safe to attempt to draw any firm conclusions from these calculations regarding the sign of $I_1(0, \infty)$. The question of whether or not the effects of second helium ionization are sufficiently large to produce pulsational instability has therefore not been answered in this investigation, although they have been shown to be a significant destabilizing influence.

It can be shown from the analytic theory that the values of $|I_1(0, z_1)|$ would have been increased over their present values if $\mathfrak{H}_{1,a}$ had remained approximately constant and equal to its minimum value at all points exterior to point a in Figures 1 and 2 (cf. Secs. IV, *a* and *b*). It is estimated that the increase might have been between, say, 5 and 20 per cent, depending on the radius. The corresponding values of $I_1(z_1, \infty)$ would hardly have been affected at all (cf. last paragraph in Sec. IV, *a*). Since the present values of $|I_1(0, z_1)|$ are already almost large enough to produce instability, it is likely that the computed values of $I_1(0, \infty)$ would in this case have been negative for some values of $\log R$.

We note, next, that, for $\log L = 3.13$, the minimum values of $I_1(0, \infty)$ for $B = 0.15$ are roughly equal to those for $B = 0.25$, while those for $B = 0.05$ are several times larger than those for either $B = 0.15$ or $B = 0.25$. This implies that the question of pulsational instability is not very sensitive to the value of B, provided that B is larger than some value which lies between, say, 0.05 and 0.10. For $B = 0$, it may be inferred that the envelopes would have had no destabilizing influence and would have contributed to the pulsational stability of the star.

While the sign of I_1 (0, ∞) cannot be determined reliably from the present calculations, it is encouraging to note that I_1 (0, ∞) actually attains a minimum with respect to R for $\log L = 3.13$, for the two cases $B = 0.05$ and $B = 0.15$; a minimum would probably have been reached also for $B = 0.25$ if the calculations for this case had been extended to larger values of $\log R$. The dependence on R, however, is discouragingly uncritical. Also, for $\log L = 4.13$ and $B = 0.15$, I_1 (0, ∞) decreases monotonically with R in the range that was covered by the integrations (i.e., the range of reasonable values of R). The results for this latter case, however, may be particularly unreliable because of the relatively large values of z in the region of second helium ionization (cf. Sec. IV, *e*, and the discussion following eq. [12]).

For $\log L = 3.13$, the values of R (say $R_{\rm crit}$) at which I_1 (0, ∞) attains minimum (cf. the third column of Table 6) are seen to be larger than $R_{\rm obs}$, the observed value of R, but the discrepancy becomes smaller as B decreases. Adopting $\log R_{\rm crit} = 1.777$ for $B = 0.25$ ($\log L = 3.13$), we have $R_{\rm crit}/R_{\rm obs} = 1.22$, 1.59, and 1.84 for $B = 0.05$, 0.15, and 0.25, respectively.

The general conclusion to be drawn from this subsection is that, while the precise numerical results of the stability calculations cannot be trusted because of the lack of interiors and the numerous approximations made, there does exist a definite destabilizing influence due to second helium ionization in the envelopes, one that is strong enough to be a significant factor in determining the over-all stability of the star. Moreover, the pulsational instability attains maximum (at least for $\log L = 3.13$) for values of R which are at least reasonable, if not in close agreement with observation.

It may also be inferred from the calculations that if either first helium ionization or hydrogen ionization had been invoked as the source of the instability, rather than second helium ionization, only a negligible destabilizing influence would have resulted, except possibly for values of R so large as to lie completely outside the range of the classical cepheids.

d) Discussion of ϕ^*

Arguments were presented in N-AI for associating maximum pulsational instability with a value of about unity for ϕ^*, the value of $\phi(z)$ (cf. eq. [37]) at the level (z^*) of 50 per cent ionization of the critical element responsible for the instability. This was, in fact, the basis of the derivation of the semitheoretical II-L relations of Papers IV and V. The present calculations permit making a partial check of this assumption.

To summarize briefly the ideas underlying the derivation of the II-L relations of Papers IV and V: Let ϕ_c denote the value of ϕ^* at which the instability against pulsation attains maximum. Assuming that the condition of maximum instability is also a condition for pulsation, this latter condition, then, is that

$$\phi^* = \phi_c \ , \tag{59}$$

where ϕ_c is a constant whose value is assumed to be near unity. For a star evolving with constant L and M, ϕ^* (R) depends rather critically on R; it was shown in Paper V that $\phi^* \propto R^\beta$, where $\beta = 2.5$ (the present calculations give, incidentally, a mean value of $\beta \approx 2.2$ for the radiative envelope models). If $R_{\rm crit}$ is the value of R for which equation (59) is satisfied, then $R_{\rm crit}$ (which would then be the theoretical equilibrium radius of a cepheid with given L and M) is given by the solution of the equation

$$\phi^* (R_{\rm crit}) = \phi_c \ . \tag{60}$$

The period of pulsation, corresponding to $R = R_{\rm crit}$, is then obtained from the period–mean-density relation (cf. eq. [15*a*]). The assumption of constancy of ϕ_c was shown in Papers IV and V to lead to II-L relations whose slopes were in good agreement with that of the empirical II-L relation (cf. eq. [50]). The values of ϕ_c required to yield $R_{\rm crit} =$

R_{obs} (for classical cepheids), assuming He^+ to be the critical constituent responsible for the instability, were 1.0 for the convective envelopes of Paper IV and 0.44 for the radiative envelopes of Paper V (for $B = 0.15$).

In Table 6 are given the values of $\log R_{crit}$ and ϕ^* (R_{crit}) as obtained from the present calculations (cf. Fig. 5), for three values of B, for the case $\log L = 3.13$, $\log M = 0.73152$, $n = 0.70$, $s = 2.10$, and $Q_d = 0.04$. Here T^* denotes the temperature at the level of 50 per cent He^+ ionization. Because of time limitations, the integrations for $B = 0.25$ were not actually carried to $R = R_{crit}$, so the value of R_{crit} given in Table 6 is based on a rough extrapolation of the curve given in Figure 5 for this case. Parentheses about the entries in Table 6 denote uncertainty arising from this extrapolation.

It is seen from the entries in Table 6 that the values of ϕ^* (R_{crit}) are all very nearly the same for the three rather widely different values of B that were used. While definite minima in I_1 (0, ∞) were actually obtained only for the two cases shown in the first two rows of Table 6, the near constancy of ϕ^* (R_{crit}) for these two cases does lend some support to the validity of the assumption that ϕ^* (R_{crit}) = const. is a condition for pulsational instability. The values of ϕ^* (R_{crit}) are also seen to be near unity, as was assumed in Papers IV and V. The present calculations suggest that the critical value of ϕ^* required for instability may be $\phi_c \approx 1.5$ or 1.6.

TABLE 6

$\phi^*(R_{crit})$ AS FUNCTION OF B

(n=0.70, s=2.10, Q_d=0.04, log L=3.13, log M=0.73152)

B	T^*(° K)×10^{-3}	log R_{crit}	$\phi^*(R_{crit})$
0.05.....	46.0	1.599	1.55
.15.....	43.7	1.714	1.57
0.25.....	42.7	(1.777)	(1.69)

Because minima in I_1 (0, ∞) were obtained for only one value of $\log L$, a theoretical Π-L relation cannot be derived directly on the basis of the stability calculations. If, however, we accept the constancy of ϕ^* (R_{crit}) and adopt, say, $\phi_c = 1.5$, we can derive a Π-L relation by the same methods that were used in Papers IV and V. The result is a curve that is nearly parallel to the empirical curve and which is displaced, for given L, toward longer periods by $\Delta \log \Pi \approx 0.302$ for $B = 0.15$.

Finally, the present calculations permit an estimate to be made of the value of the quantity $\langle m \rangle$, which was defined in Papers IV and V and whose value was assumed in both these papers to be 3. Since the present calculations of ϕ^* include the effects of curvature, $\langle m \rangle$ must be defined slightly differently than was done in Papers IV and V. We shall here define $\langle m \rangle$ in such a way that equations (8) and (9) in Paper V are still valid. Then $\langle m \rangle$ is determined by the equations

$$\frac{1}{\langle m \rangle} = \frac{2}{3}\left\langle \frac{x^4}{\Lambda \Theta_{T^\mu}} \right\rangle, \tag{61a}$$

$$\left\langle \frac{x^4}{\Lambda \Theta_{T^\mu}} \right\rangle \int_0^{P^*} P^{1/(n_e+1)} dP = \int_0^{P^*} \frac{x^4 P^{1/(n_e+1)}}{\Lambda \Theta_{T^\mu}} dP, \tag{61b}$$

where the notation is the same as in Paper V. Thus $\langle m \rangle$ depends on z^* as well as on B and on the mechanism of energy transfer.

For $B = 0.15$, the values of $\langle m \rangle$ for several models ranged between about 1.8 and 2.2, with a mean value of about 2.0.

e) The Effects of Varying n, s, and Q

We may summarize the effects of varying n, s, and Q by the following qualitative remarks:

1. Variation in the values of n and s over reasonable ranges produced changes in the detailed quantitative results, but it introduced no qualitatively new or significant features.

2. Most of the results were found to be rather sensitive to the value used for Q. The immediate effect of varying Q is to alter the behavior of y, the relative pulsation amplitude (cf. eq. [12]), the relative magnitude of the alteration increasing with depth. Without interiors to fix the value of Q, then, it follows that all quantities which depend on y and its derivatives are subject to this inherent source of uncertainty. Unreasonable values of Q may be excluded by the condition that y (in the fundamental mode) decrease monotonically inward through the envelopes without vanishing. Since y behaved in this manner (at least for the population I cepheids) with the value of Q_d (i.e., 0.04) that was used in most of the calculations, then this semiempirical value is evidently not unreasonable from the standpoint of the mathematical characteristics of the envelopes.

Within the realm of reasonable values of Q, however, there still exists a rather wide range of possible curves for y (z). Because all these curves are normalized to unity at $z = 0$ and because the effects of the uncertainty in the value of Q increase with depth, it follows that the results based on the present method of treatment of the adiabatic problem (cf. Sec. II, *b*) decrease in reliability rather rapidly with depth.

V. CONCLUSIONS

It may be concluded that the results of these calculations, taken at face value, are favorable in the following respects to the helium-ionization hypothesis, at least as applied to the population I cepheids:

1. The calculations show that second helium ionization, occurring at a critical depth in the envelope, can, with a reasonable helium abundance, incite a strong tendency toward pulsational instability, at least for the kinds of envelopes that were considered here. First helium ionization and hydrogen ionization can be ruled out as *primary* causative agents in producing instability because they occur at depths (in ϕ-measure) which are too small for them to be directly effective for radii in the cepheid region and for the kinds of envelopes considered here.

2. For radii near the observed values, the negative dissipation (produced by second helium ionization) in the envelopes is comparable in magnitude to the estimated positive dissipation in the interiors (cf. Sec. IV, *c*). The theoretical possibility of pulsational instability arising from this source is therefore at least not excluded by these calculations. However, before a definitive answer can be given to the question of the existence of pulsational instability, information from the interiors will be needed. While the possession of suitable interior models for cepheids of both populations would be highly desirable for this purpose as well as for other reasons, it is possible that complete interior models may not actually be required. A sufficiently precise answer to the stability question might be provided merely by adopting a different computational procedure and pushing the integrations to considerably greater depths than those that were attained in this investigation.[2] For this purpose only a very rough interior model would probably be sufficient.

3. *Maximum* pulsational instability occurs, at least for the models with log L (solar units) = 3.13, for radii which are reasonable, if not in close agreement with observation. For B (helium/hydrogen ratio, by numbers) = 0.15, the radius corresponding to maximum instability is larger than the empirical radius by a factor of about 1.6. In addition, the critical value of the phase-lag function corresponding to maximum instability is about 1.5 or 1.6 (cf. Sec. IV, *d*).

[2] The author is indebted to Dr. M. Schwarzschild for this suggestion.

4. The relative amplitudes and phases of the surface flux variations, for reasonable radii and helium abundances, are, in a very rough sense, consistent with observations of cepheids. For $B = 0.15$ and $\log L = 3.13$, the amplitude of the light-variations is about $0^m.7$ or $0^m.8$, and the phase lag (relative to minimum radius) is about 40° or 50° for radii near the observed values. It must be borne in mind that a linear theory, even at best, should not necessarily be expected to yield closely realistic results regarding details of surface flux variations, etc. (see Ledoux and Walraven 1958, p. 505, in this connection).

Furthermore, it has been shown that inclusion of first helium ionization and hydrogen ionization would have increased the magnitude of the pulsational instability (through indirect effects) and would have brought the surface flux variations into even closer correspondence with observations than the present calculations show. The effect of these additional ionizations on the radii for which maximum instability is attained cannot be ascertained without further calculations.

It is clear that a more refined discussion of the envelopes of the population II cepheids will be required before these stars can be placed unambiguously in the same scheme that applies to the population I cepheids. It is possible that a revision of ideas regarding the physical mechanism responsible for the instability in these stars will be required. Moreover, a nonlinear theory may be needed to treat adequately the population II cepheids.

The most important source of uncertainty in the calculations described here is perhaps the question of the accuracy of the Woltjer method in the first approximation in the solution of the non-adiabatic problem. This question may be answered, for example, either by carrying out higher approximations within the Woltjer scheme or by adopting a different approach based on an exact numerical solution of the entire set of linearized pulsation equations (a system of the eighth order). This latter approach is now under investigation by the author.[3] It is interesting to note that the behavior of the surface flux variations was in qualitative agreement with results anticipated earlier (cf. N-AI) on the basis of a somewhat different (and cruder) treatment of the non-adiabatic problem. In addition, the inference that phase leads would occur in our case $B = 0$ is in agreement with results reported by Zhevakin (1954*b*) for a physically similar case. These considerations suggest that the results obtained by use of the Woltjer method in the first approximation are not likely to be, qualitatively at least, grossly in error. Until a definitive answer to this question has been given, however, the present results must be regarded as highly tentative and preliminary.

The author wishes to express his gratitude to Dr. Fred L. Whipple, who made it possible for the bulk of this work to be carried out at the Smithsonian Astrophysical Observatory during the summer of 1959; to Dr. Charles A. Whitney for his indorsement of and interest in this work, his encouragement, and a number of enlightening discussions; and to Mr. R. Thomas Giuli, who did all the programing for the project, both for the 650 and for the 704, and whose tireless assistance throughout the entire project was a major factor in its completion. The author is also grateful to Dr. Martin Schwarzschild, who, while acting as referee for this paper, offered suggestions some of which played an important role in the preparation of the final manuscript; and to Professor Marshal H. Wrubel for additional suggestions.

The author wishes, in addition, to express his indebtedness to Mr. Richard C. Lesser for making available to him the facilities of the Cornell Computing Center for carrying

[3] The exact numerical solutions of the complete eighth order system of linearized pulsation equations, as applied to envelope models of the same kind as those considered in this paper, have recently (July, 1960) been obtained by the author during a brief tenure at the Smithsonian Astrophysical Observatory in Cambridge, Massachusetts. It may be concluded from the exact calculations that the results obtained by use of the Woltjer method in the first approximation are, indeed, qualitatively correct and that they do not differ greatly, quantitatively, from the exact results. The detailed results obtained and the method of calculation used in the exact treatment will be described in a future paper.

out some of the preliminary stages of the investigation. Finally, support of certain phases of this work, provided by a grant from Research Corporation, is gratefully acknowledged.

REFERENCES

Cox, J. P. 1958, *Ap. J.*, **127**, 194.
———. 1959, *ibid.*, **130**, 296.
Cox, J. P., and Whitney, C. A. 1958, *Ap. J.*, **127**, 561.
Eddington, A. S. 1927, *M.N.*, **87**, 539.
Forsyth, A. R. 1929, *A Treatise on Differential Equations* (6th ed.; New York: St Martin's Press), chap. iv.
Hoyle, F., and Schwarzschild, M. 1955, *Ap. J. Suppl.*, Vol. **2**, No. 13, Sec. VI.
Kuiper, G. P. 1938, *Ap. J.*, **88**, 429.
Ledoux, P., and Walraven, Th. 1958, *Hdb. d. Phys.* (Berlin: Springer-Verlag), ed. S. Flügge, Vol. **51**.
Rosseland, S. 1949, *The Pulsation Theory of Variable Stars* (Oxford: Clarendon Press).
Sandage, A. 1958, *Ap. J.*, **127**, 513.
Schwarzschild, M. 1958, *Structure and Evolution of the Stars* (Princeton: Princeton University Press).
Stebbins, J., and Kron, G. E. 1957, *Ap. J.*, **126**, 266.
Unsöld, A. 1955, *Physik der Sternatmosphären* (2d ed.; Berlin: Springer-Verlag), pp. 227–228.
Watson, G. N. 1944, *A Treatise on the Theory of Bessel Functions* (2d ed.; Cambridge: Cambridge University Press), chap. iii.
Whitehead, C. S. 1911, *Quart. J. Math.*, **42**, 316.
Woltjer, J. 1936, *B.A.N.*, **8**, 17.
Zhevakin, S. A. 1953, *Russ. A. J.*, **30**, 161.
———. 1954*a*, *ibid.*, **31**, 141.
———. 1954*b*, *ibid.*, p. 335.
———. 1958, *Soviet Astr. J.*, **2**, 538.
———. 1959, *Russ. A. J.*, **36**, 394.